

# Power Corrections in the Decay Rate and Distributions in $B \rightarrow X_s \ell^+ \ell^-$ in the Standard Model

**A. Ali<sup>\*</sup>, G. Hiller<sup>†</sup>,**  
Deutsches Elektronen-Synchroton DESY, Hamburg

**L.T. Handoko<sup>‡</sup>, and T. Morozumi<sup>§</sup>**  
Department of Physics, Hiroshima University  
1-3-1 Kagamiyama, Higashi Hiroshima - 739, Japan

## Abstract

We investigate the leading power corrections to the decay rates and distributions in the decay  $B \rightarrow X_s \ell^+ \ell^-$  in the standard model (SM) using heavy quark expansion (HQE) in  $(1/m_b)$  and a phenomenological model implementing the Fermi motion effects of the  $b$  quark bound in the  $B$  hadron. In the HQE method, we find that including the leading power corrections the decay width  $\Gamma(B \rightarrow X_s \ell^+ \ell^-)$  decreases by about 4% and the branching ratio  $\mathcal{B}(B \rightarrow X_s \ell^+ \ell^-)$  by about 1.5% from their (respective) parton model values. The dilepton invariant mass spectrum is found to be stable against power corrections over a good part of this spectrum. However, near the high-mass end-point this distribution becomes negative with the current value of the non-perturbative parameter  $\lambda_2$  (the  $\lambda_1$ -dependent corrections are found to be inoccous), implying the breakdown of the HQE method in this region. Our results are at variance with the existing ones in the literature in both the decay rate and the invariant dilepton mass distribution calculated in the HQE approach. As an alternative, we implement the non-perturbative effects in the decay  $B \rightarrow X_s \ell^+ \ell^-$  using a phenomenologically motivated Gaussian Fermi motion model. We find small corrections to the branching ratio, but the non-perturbative effects are perceptible in both the dilepton mass distribution and the Forward-Backward asymmetry in the high dilepton mass region. Using this model for estimating the non-perturbative effects, modeling the dominant long distance (LD) contributions from the decays  $B \rightarrow X_s + (J/\psi, \psi', \dots) \rightarrow X_s \ell^+ \ell^-$ , and taking into account the next-to-leading order perturbative QCD corrections in  $b \rightarrow s \ell^+ \ell^-$ , we present the decay rates and distributions for the inclusive process  $B \rightarrow X_s \ell^+ \ell^-$  in the SM.

---

<sup>\*</sup>E-mail address: ali@x4u2.desy.de

<sup>†</sup>E-mail address: ghiller@x4u2.desy.de

<sup>‡</sup>On leave from P3FT-LIPI, Indonesia. E-mail address: handoko@theo.phys.sci.hiroshima-u.ac.jp

<sup>§</sup>E-mail address: morozumi@theo.phys.sci.hiroshima-u.ac.jp

# 1 Introduction

Rare  $B$  decays  $B \rightarrow X_s \ell^+ \ell^-$  and  $B \rightarrow X_s \gamma$  are well suited to test the SM and search for physics beyond the SM. In the SM, such processes are governed by the Glashow-Iliopoulos-Maiani (GIM) mechanism [1], and their rates and distributions are sensitive to the top quark mass and the Cabibbo-Kobayashi-Maskawa (CKM) matrix elements [2]. First measurements of the decay rates for the exclusive decay  $B \rightarrow K^* + \gamma$  [3] and the inclusive decay  $B \rightarrow X_s \gamma$  [4] have been reported by the CLEO collaboration. At the partonic level, the complete leading order (LO) anomalous dimension matrix involving the  $b \rightarrow s \gamma$  decay was calculated in [5]-[7] in the context of an effective five-quark theory. First calculations of the gluon bremsstrahlung and virtual corrections, which are part of the next-to-leading-order perturbative QCD improvements, were reported in [8]-[10] (see also [11, 12]). The NLO virtual corrections to the matrix elements have been completed in [13]. A first calculation of the hitherto missing NLO anomalous dimension matrix has been recently reported in [14]. Leading power corrections in  $(1/m_b)$  to the decay rate  $\Gamma(B \rightarrow X_s \gamma)$  (and  $\Gamma(B \rightarrow X \ell \nu_\ell)$ , which is often used to estimate the branching ratio  $\mathcal{B}(B \rightarrow X_s \gamma)$ ) have also been calculated in the heavy quark expansion (HQE) approach [15, 16]. A quantitative measure of the rapport between experiment and present estimates in the SM is the CKM matrix element ratio  $|V_{ts}|/|V_{cb}|$  for which a value  $|V_{ts}|/|V_{cb}| = 0.85 \pm 0.12$  (expt)  $\pm 0.10$  (th) has been obtained from the inclusive decay rate for  $B \rightarrow X_s \gamma$  [17], in agreement with the bounds obtained from unitarity of the CKM matrix [18].

It is known that the inclusive energy spectra in the decays  $B \rightarrow X \ell \nu_\ell$  and  $B \rightarrow X_s \gamma$  are not entirely calculable in the HQE framework [16],[19]-[21]. In particular, the end-point energy spectra are problematic in that the energy released for the light quark system in the decay  $b \rightarrow qX$  (here  $X = \gamma$  or a dilepton pair) is not of order  $m_b$  but of order  $\bar{\Lambda}$ , where  $\bar{\Lambda} = m_B - m_b = O(\Lambda_{\text{QCD}})$ . Hence, the expansion parameter in the HQE approach, which is formally of  $O(1/Q^2) = O(1/m_b^2)$ , near the end-point gets replaced by a quantity which is of  $O(1/K^2) = O(1/\bar{\Lambda} m_b) \ll O(1/m_b^2)$ , implying the onset of the breakdown of the HQE method. To make contact with experiments one has to smear the energy spectrum in question over an energy interval sufficiently larger than  $\Lambda_{\text{QCD}}$ . Thus, direct comparison of theoretical distributions with experiments requires additional input in terms of phenomenological models, e.g., the Gaussian Fermi-motion model of [22], which incorporate such smearing. The smearing effects

are very important in  $B \rightarrow X_s \gamma$  [8, 9, 12] and not negligible in the lepton and hadron-energy spectra in the decays  $B \rightarrow X_c(X_u) \ell \nu_\ell$ , either [22]-[24]. Alternatively, one may have to resort to a resummation of the power corrections near the end-point [19, 25]. Such resummations, however, remain so far inconclusive.

In this paper, we address the related FCNC process  $B \rightarrow X_s \ell^+ \ell^-$ ,  $\ell = e, \mu$ . (Since we neglect the lepton masses in our calculation, our results are not applicable to the decay  $B \rightarrow X_s \tau^+ \tau^-$ .) The SM-based short distance (SD) contribution to the decay rate for the partonic process  $b \rightarrow s \ell^+ \ell^-$ , calculated in the free quark decay approximation, has been known in the LO approximation for some time [26]. In the meanwhile, also the NLO perturbative QCD corrections have been calculated which reduce the scheme-dependence of the LO effects in these decays [27, 28]. In addition, long distance (LD) effects, which are expected to be very important in the decay  $B \rightarrow X_s \ell^+ \ell^-$  [29], have been estimated from data on the premise that they arise dominantly from the charmonium resonances  $J/\psi$  and  $\psi'$  through the decay chains  $B \rightarrow X_s J/\psi(\psi') \rightarrow X_s \ell^+ \ell^-$ . Higher resonances ( $\psi'', \psi''', \dots$ ) also contribute though at a reduced level. Estimates of the LD effects away from the resonance regions involve specific assumptions about the  $q^2$ -dependence of the relevant vertices, which at present can only be obtained in specific models [29] - [32].

The particular aspect we are interested in is an estimate of the non-perturbative effects on the decay distributions in  $B \rightarrow X_s \ell^+ \ell^-$ , which take into account the  $B$ -hadron wave function effects and incorporate the physical threshold in the final state on the underlying partonic calculations. This effects both the SD- and LD-contributions, and to the best of our knowledge has not yet been calculated. Closely related to this aspect is the question of power corrections to the parton model decay rates and spectra which have been calculated for the SD-part of the dilepton invariant mass distribution in  $B \rightarrow X_s \ell^+ \ell^-$  by Falk, Luke and Savage [33] (henceforth this paper is referred to as FLS) using the HQE approach. We reevaluate these corrections in this paper, reaching different results and conclusions than in the FLS paper which we specify later.

From the power corrections calculated in the HQE approach for the decays  $B \rightarrow X_s \gamma$  and  $B \rightarrow X \ell \nu_\ell$  [15, 16], we recall that there are no leading, i.e.,  $O(1/m_b)$ , corrections in the inclusive rates. Likewise, in the decay  $B \rightarrow X_s \ell^+ \ell^-$ , the first non-vanishing corrections to the inclusive

rates are of  $O(1/m_b^2)$ . Furthermore, the dilepton mass spectrum in  $B \rightarrow X_s \ell^+ \ell^-$  is found to be well behaved in the HQE framework in the *entire* dilepton mass range in FLS [33]. In particular, the high dilepton invariant mass spectrum in the parton model is found to receive moderate power corrections, typically  $O(10\%)$ , increasing the dilepton yield in  $B \rightarrow X_s \ell^+ \ell^-$  (see Fig. 2 in [33]). This result differs qualitatively from analogous power corrections in the lepton energy spectra in  $B \rightarrow X \ell \nu_\ell$ , which are large and negative near the end-points (see, for example, Figs. 5 - 8 in the paper by Manohar and Wise [16]). In addition, taking the  $V - A$  limit in the matrix element for  $B \rightarrow X_s \ell^+ \ell^-$ , the differential distributions and decay rate in this process can be related to the corresponding quantities in the semileptonic decay  $B \rightarrow X \ell \nu_\ell$ . The power corrections in the latter decays have been calculated and discussed at great length by Bigi et al. in [15] and by Manohar and Wise [16]. We are of the opinion that both the power corrected dilepton spectrum and the inclusive decay rate  $\Gamma(B \rightarrow X_s \ell^+ \ell^-)$  obtained by integrating this spectrum in FLS are at variance with the results in [15, 16] in this limit (see Appendix C). In view of the impending interest in the decay  $B \rightarrow X_s \ell^+ \ell^-$ , in particular the dilepton mass spectrum and the Forward-backward asymmetry involving  $\ell^+$  versus  $\ell^-$  [34], which have been put forward as precision test of the SM in the FCNC sector and hence a possible place for discovering new physics [35, 36], we have recalculated the power corrections in this process in the SM using the HQE approach.

To that end, we have computed the Dalitz distribution,  $d^2\mathcal{B}/d\hat{s}d\hat{u}$ , for the decay  $B \rightarrow X_s \ell^+ \ell^-$  (see section 2 for the definition of these variables), taking into account the NLO perturbative QCD correction in  $\alpha_s$  and the leading  $1/m_b$  corrections in the HQE approach. In doing this, we have also kept the  $s$ -quark mass effects. Integrating over one of the variables, the resulting expressions for the dilepton invariant mass and the FB asymmetry are derived. While the power-corrected FB asymmetry in  $B \rightarrow X_s \ell^+ \ell^-$  is a new result, not presented earlier, our expression for the power-corrected dilepton mass distribution is not in agreement with the one presented in FLS [33]. Since the derivations of the final results for  $d\Gamma(B \rightarrow X_s \ell^+ \ell^-)/d\hat{s}$  and the FB asymmetry  $\mathcal{A}(\hat{s})$  are rather involved, we have decided to give the details of the calculations so that they can be checked stepwise and the source of this discrepancy pinned down accordingly. Some checks of our results in the limiting case mentioned above are already possible and have been carried out. In particular, we are able to derive the results in [15, 16]

taking the appropriate limit of our expressions in  $B \rightarrow X_s \ell^+ \ell^-$  (see again Appendix c).

We find that the final-state distributions in  $B \rightarrow X_s \ell^+ \ell^-$  are not calculable entirely in the HQE approach, as the dilepton mass distribution becomes negative in the end-point region. While this defect may be resuscitated by resummation of the HQE-power corrections, we do not attempt this here. Instead, we estimate the non-perturbative effects on the decay rates and distributions in  $B \rightarrow X_s \ell^+ \ell^-$  by invoking the Gaussian Fermi motion model [22]. This model has been used successfully in the analysis of the lepton energy spectrum in the semileptonic decays  $B \rightarrow X \ell \nu_\ell$  [23] and the photon energy spectrum in  $B \rightarrow X_s \gamma$  [9]. As pointed out in [16] on the example of  $B \rightarrow X \ell \nu_\ell$ , this model reproduces the effect due to the kinetic energy term  $\lambda_1$  in the HQE approach, if the  $b$ -quark mass is appropriately defined, but there is no analogue of  $\lambda_2$  (the matrix element of the magnetic moment operator) in the Fermi motion model. The distributions in the two approaches (HQE and the Fermi motion model) are hence, in general, different, which is most noticeable near the end-points. By construction, there are no negative probabilities encountered in the Fermi motion model and the final state thresholds can be correctly incorporated.

This paper is organized as follows: In section 2, we derive the double differential distribution  $d^2\mathcal{B}/d\hat{s}d\hat{u}$  for the decay  $B \rightarrow X_s \ell^+ \ell^-$ , including the explicit  $O(\alpha_s)$  and the leading power corrections in  $1/m_b$ , giving in Appendix A the individual contributions to the structure functions from several contributing sources governing these decays. Some of the lengthy expressions obtained in the derivation of the HQE-improved Dalitz distribution are displayed in Appendix B. The power-corrected dilepton invariant mass distribution and the FB asymmetry in  $B \rightarrow X_s \ell^+ \ell^-$ , together with their simplified versions in the limit  $m_s = 0$ , are also given in this section. We also present here numerical comparisons in the two quantities of interest between the parton model and the HQE-approaches, as well as differences between our result and the one in FLS [33]. In Appendix C, we present the limiting case of our results for  $B \rightarrow X_s \ell^+ \ell^-$  and compare them with the existing ones in the literature [15, 16]. In Appendix D, we show (a peripheral result) that the energy asymmetry defined in [36] and the FB asymmetry introduced in [34] are related. In section 3, we implement the  $B$ -meson wave function effects and the physical threshold on the final state in  $B \rightarrow X_s \ell^+ \ell^-$ , using the NLO-corrected parton distributions and the Gaussian Fermi motion model [22]. Since the calculation of the FB asymmetry in this model

involves some non-trivial kinematic transformations, we have given the details in Appendix E. The LD-contributions in  $B \rightarrow X_s \ell^+ \ell^-$  are estimated in section 4, using data on vector meson intermediate states  $B \rightarrow V + X_s$ , where  $V = (J/\psi(1S), \dots, \psi(6S))$ . The resulting dilepton mass spectrum and the FB asymmetry, including the wave-function and LD-effects, are also presented here. We conclude with a discussion of our results and possible improvements of the LD-effects in  $B \rightarrow X_s \ell^+ \ell^-$  in section 5.

## 2 Power corrections to the dilepton invariant mass distribution and FB asymmetry in $B \rightarrow X_s \ell^+ \ell^-$

We start by defining the various kinematic variables in the decay  $b(p_b) \rightarrow s(p_s) + \ell^+(p_+) + \ell^-(p_-)$ .

$$\begin{aligned} u &= -(p_b - p_+)^2 + (p_b - p_-)^2, \\ s &= (p_+ + p_-)^2, \\ u(s, m_s) &= \sqrt{(s - (m_b + m_s)^2)(s - (m_b - m_s)^2)}. \end{aligned} \quad (1)$$

For subsequent use, we note that  $p_{\pm} = (E_{\pm}, \mathbf{p}_{\pm})$ , and  $q_{\mu} = (p_+ + p_-)_{\mu}$  is the momentum transfer to the lepton-anti-lepton pair (hence  $q^2 = s$ ). We also define the four-velocity of the  $b$  quark,  $v_{\mu} = (p_b)_{\mu}/m_b$ , which we shall take subsequently to be the same as that of the  $B$  hadron,  $v_{\mu} = (p_B)_{\mu}/M_B$ . Finally, we introduce the scaled variables  $\hat{s}$  and  $\hat{u}$

$$\begin{aligned} \hat{s} &= \frac{s}{m_b^2}, \\ \hat{u} &= \frac{u}{m_b^2} = 2v \cdot (\hat{p}_+ - \hat{p}_-), \end{aligned} \quad (2)$$

which in the decay  $b \rightarrow s \ell^+ \ell^-$  are bounded as follows,

$$\begin{aligned} -\hat{u}(\hat{s}, \hat{m}_s) &< \hat{u} < +\hat{u}(\hat{s}, \hat{m}_s), \\ \hat{u}(\hat{s}, \hat{m}_s) &= \sqrt{[\hat{s} - (1 + \hat{m}_s)^2][\hat{s} - (1 - \hat{m}_s)^2]}, \\ 4\hat{m}_l^2 &< \hat{s} < (1 - \hat{m}_s)^2. \end{aligned} \quad (3)$$

where  $\hat{m}_i$  and  $\hat{p}_i$  are the scaled quark masses and scaled momenta, respectively,  $\hat{m}_i = m_i/m_b$ ,  $\hat{p}_i = p_i/m_b$ .

## 2.1 NLO-corrected amplitude for $b \rightarrow s\ell^+\ell^-$ in the effective Hamiltonian approach

Next, the explicit expressions for the matrix element and (partial) branching ratios in the decays  $b \rightarrow s\ell^+\ell^-$  are presented in terms of the Wilson coefficients of the effective Hamiltonian obtained by integrating out the top quark and the  $W^\pm$  bosons,

$$\mathcal{H}_{eff}(b \rightarrow s + X) = \mathcal{H}_{eff}(b \rightarrow s + \gamma) - \frac{4G_F}{\sqrt{2}} V_{ts}^* V_{tb} [C_9 O_9 + C_{10} O_{10}], \quad (4)$$

where

$$\mathcal{H}_{eff}(b \rightarrow s + \gamma) = -\frac{4G_F}{\sqrt{2}} V_{ts}^* V_{tb} \sum_{i=1}^8 C_i(\mu) O_i(\mu). \quad (5)$$

Here,  $V_{ij}$  are the CKM matrix elements and the CKM unitarity has been used in factoring out the product  $V_{ts}^* V_{tb}$ . The operator basis is chosen to be (here  $\mu$  and  $\nu$  are Lorentz indices and  $\alpha$  and  $\beta$  are colour indices)

$$O_1 = (\bar{s}_{L\alpha} \gamma_\mu b_{L\alpha})(\bar{c}_{L\beta} \gamma^\mu c_{L\beta}), \quad (6)$$

$$O_2 = (\bar{s}_{L\alpha} \gamma_\mu b_{L\beta})(\bar{c}_{L\beta} \gamma^\mu c_{L\alpha}), \quad (7)$$

$$O_3 = (\bar{s}_{L\alpha} \gamma_\mu b_{L\alpha}) \sum_{q=u,d,s,c,b} (\bar{q}_{L\beta} \gamma^\mu q_{L\beta}), \quad (8)$$

$$O_4 = (\bar{s}_{L\alpha} \gamma_\mu b_{L\beta}) \sum_{q=u,d,s,c,b} (\bar{q}_{L\beta} \gamma^\mu q_{L\alpha}), \quad (9)$$

$$O_5 = (\bar{s}_{L\alpha} \gamma_\mu b_{L\alpha}) \sum_{q=u,d,s,c,b} (\bar{q}_{R\beta} \gamma^\mu q_{R\beta}), \quad (10)$$

$$O_6 = (\bar{s}_{L\alpha} \gamma_\mu b_{L\beta}) \sum_{q=u,d,s,c,b} (\bar{q}_{R\beta} \gamma^\mu q_{R\alpha}), \quad (11)$$

$$O_7 = \frac{e}{16\pi^2} \bar{s}_\alpha \sigma_{\mu\nu} (m_b R + m_s L) b_\alpha F^{\mu\nu}, \quad (12)$$

$$O_8 = \frac{g}{16\pi^2} \bar{s}_\alpha T_{\alpha\beta}^a \sigma_{\mu\nu} (m_b R + m_s L) b_\beta G^{a\mu\nu}, \quad (13)$$

$$(14)$$

where  $L$  and  $R$  denote chiral projections,  $L(R) = 1/2(1 \mp \gamma_5)$ , and the two additional operators involving the dileptons are:

$$\begin{aligned} O_9 &= \frac{e^2}{16\pi^2} \bar{s}_\alpha \gamma^\mu L b_\alpha \bar{\ell} \gamma_\mu \ell, \\ O_{10} &= \frac{e^2}{16\pi^2} \bar{s}_\alpha \gamma^\mu L b_\alpha \bar{\ell} \gamma_\mu \gamma_5 \ell. \end{aligned} \quad (15)$$

The Wilson coefficients are given in the literature (see, for example, [27, 28]).

With the help of the effective Hamiltonian in eq. (4) the matrix element for the decay  $b \rightarrow s\ell^+\ell^-$  can be written as,

$$\begin{aligned} \mathcal{M}(b \rightarrow s\ell^+\ell^-) = & \frac{G_F\alpha}{\sqrt{2}\pi} V_{ts}^* V_{tb} \left[ \left( C_9^{\text{eff}} - C_{10} \right) (\bar{s} \gamma_\mu L b) (\bar{l} \gamma^\mu L l) \right. \\ & + \left( C_9^{\text{eff}} + C_{10} \right) (\bar{s} \gamma_\mu L b) (\bar{l} \gamma^\mu R l) \\ & \left. - 2C_7^{\text{eff}} \left( \bar{s} i \sigma_{\mu\nu} \frac{q^\nu}{q^2} (m_s L + m_b R) b \right) (\bar{l} \gamma^\mu l) \right]. \end{aligned} \quad (16)$$

We have kept the  $s$ -quark mass term in the matrix element explicitly and this will be kept consistently in the calculation of power corrections and phase space. The above matrix element can be written in a compact form,

$$\mathcal{M}(b \rightarrow s\ell^+\ell^-) = \frac{G_F\alpha}{\sqrt{2}\pi} V_{ts}^* V_{tb} \left( \Gamma^L_\mu L^{L\mu} + \Gamma^R_\mu L^{R\mu} \right), \quad (17)$$

with

$$L^{L/R}_\mu \equiv \bar{l} \gamma_\mu L(R) l, \quad (18)$$

$$\Gamma^{L/R}_\mu \equiv \bar{s} \left[ R \gamma_\mu \left( C_9^{\text{eff}} \mp C_{10} + 2C_7^{\text{eff}} \frac{\hat{q}}{\hat{s}} \right) + 2\hat{m}_s C_7^{\text{eff}} \gamma_\mu \frac{\hat{q}}{\hat{s}} L \right] b. \quad (19)$$

We recall that the coefficient  $C_9$  in LO is scheme-dependent. However, this is compensated by an additional scheme-dependent part in the (one loop) matrix element of  $O_9$  [27, 28]. We call the sum  $C_9^{\text{eff}}$ , which is scheme-independent and enters in the physical decay amplitude given above, with

$$C_9^{\text{eff}}(\hat{s}) \equiv C_9 \eta(\hat{s}) + Y(\hat{s}). \quad (20)$$

The function  $Y(\hat{s})$  is the one-loop matrix element of  $O_9$  and is defined as [6, 28]:

$$\begin{aligned} Y(\hat{s}) = & g(\hat{m}_c, \hat{s}) (3C_1 + C_2 + 3C_3 + C_4 + 3C_5 + C_6) \\ & - \frac{1}{2} g(1, \hat{s}) (4C_3 + 4C_4 + 3C_5 + C_6) \\ & - \frac{1}{2} g(0, \hat{s}) (C_3 + 3C_4) \\ & + \frac{2}{9} (3C_3 + C_4 + 3C_5 + C_6) \\ & - \xi \frac{4}{9} (3C_1 + C_2 - C_3 - 3C_4), \end{aligned} \quad (21)$$

$$\eta(\hat{s}) = 1 + \frac{\alpha_s(\mu)}{\pi} \omega(\hat{s}). \quad (22)$$

Here,  $\xi$  is dependent on the dimensional regularization scheme [27, 28], with

$$\xi = \begin{cases} 0 & (\text{NDR}), \\ -1 & (\text{HV}), \end{cases} \quad (23)$$

in the naive dimensional regularization (NDR) and the 't Hooft-Veltman (HV) schemes. The function  $\omega(\hat{s})$  represents the  $O(\alpha_s)$  correction from the one-gluon exchange in the matrix element of  $O_9$  [37]:

$$\begin{aligned} \omega(\hat{s}) = & -\frac{2}{9}\pi^2 - \frac{4}{3}\text{Li}_2(\hat{s}) - \frac{2}{3}\ln\hat{s}\ln(1-\hat{s}) - \frac{5+4\hat{s}}{3(1+2\hat{s})}\ln(1-\hat{s}) \\ & - \frac{2\hat{s}(1+\hat{s})(1-2\hat{s})}{3(1-\hat{s})^2(1+2\hat{s})}\ln\hat{s} + \frac{5+9\hat{s}-6\hat{s}^2}{6(1-\hat{s})(1+2\hat{s})}. \end{aligned} \quad (24)$$

The function  $g(z, \hat{s})$  includes the charm quark-antiquark pair contribution [27, 28]:

$$\begin{aligned} g(z, \hat{s}) = & -\frac{8}{9}\ln\left(\frac{m_b}{\mu}\right) - \frac{8}{9}\ln z + \frac{8}{27} + \frac{4}{9}y - \frac{2}{9}(2+y)\sqrt{|1-y|} \\ & \times \left[ \Theta(1-y)\left(\ln\frac{1+\sqrt{1-y}}{1-\sqrt{1-y}} - i\pi\right) + \Theta(y-1)2\arctan\frac{1}{\sqrt{y-1}} \right], \end{aligned} \quad (25)$$

$$g(0, \hat{s}) = \frac{8}{27} - \frac{8}{9}\ln\left(\frac{m_b}{\mu}\right) - \frac{4}{9}\ln\hat{s} + \frac{4}{9}i\pi, \quad (26)$$

where  $y = 4z^2/\hat{s}$ . With the help of the above expressions, the differential decay width becomes,

$$d\Gamma = \frac{1}{2M_b} \frac{G_F^2 \alpha^2}{2\pi^2} |V_{ts}^* V_{tb}|^2 \frac{d^3 \mathbf{p}_+}{(2\pi)^3 2E_+} \frac{d^3 \mathbf{p}_-}{(2\pi)^3 2E_-} \left( W_{\mu\nu}^L L^{L\mu\nu} + W_{\mu\nu}^R L^{R\mu\nu} \right), \quad (27)$$

where  $W_{\mu\nu}$  and  $L_{\mu\nu}$  are the hadronic and leptonic tensors, respectively. The hadronic tensor  $W_{\mu\nu}^{L/R}$  is related to the discontinuity in the forward scattering amplitude, denoted by  $T_{\mu\nu}^{L/R}$ , through the relation  $W_{\mu\nu} = 2\text{Im } T_{\mu\nu}$ . Transforming the integration variables to  $\hat{s}$ ,  $\hat{u}$  and  $v \cdot \hat{q}$ , one can express the Dalitz distribution in  $b \rightarrow s\ell^+\ell^-$  (neglecting the lepton masses) as:

$$\frac{d\Gamma}{d\hat{u} d\hat{s}} = \frac{1}{2m_b} \frac{G_F^2 \alpha^2}{2\pi^2} \frac{m_b^4}{256\pi^4} |V_{ts}^* V_{tb}|^2 2\text{Im} \int d(v \cdot \hat{q}) \left( T_{\mu\nu}^L L^{L\mu\nu} + T_{\mu\nu}^R L^{R\mu\nu} \right), \quad (28)$$

with

$$T_{\mu\nu}^{L/R} \equiv i \int d^4x e^{-i\hat{q} \cdot x} \left\langle B \left| T \left\{ \Gamma_{1\mu}^{L/R}(x), \Gamma_{2\nu}^{L/R}(x) \right\} \right| B \right\rangle, \quad (29)$$

$$\begin{aligned} L^{L/R\mu\nu} \equiv & \sum_{\text{spin}} \left[ \bar{v}^{L/R}(p_+) \gamma^\mu u^{L/R}(p_-) \right] \left[ \bar{u}^{L/R}(p_-) \gamma^\nu v^{L/R}(p_+) \right] \\ = & 2 \left[ p_+^\mu p_-^\nu + p_-^\mu p_+^\nu - g^{\mu\nu} (p_+ \cdot p_-) \mp i\epsilon^{\mu\nu\alpha\beta} p_{+\alpha} p_{-\beta} \right], \end{aligned} \quad (30)$$

where  $\Gamma_{1\mu}^{L/R\dagger} = \Gamma_{2\mu}^{L/R} = \Gamma_\mu^{L/R}$ , given in eq. (19). The Dalitz distribution eq. (28) contains the explicit  $O(\alpha_s)$ -improvement, and the two distributions in which we are principally interested in can be obtained by straight-forward integrations.

## 2.2 Leading power ( $1/m_b$ ) corrections in the decay $B \rightarrow X_s \ell^+ \ell^-$

The next task is to expand the forward scattering amplitude  $T_{\mu\nu}$  in the inverse powers in  $1/m_b$ . Suppressing the Lorentz indices for the time being, this expansion can be formally represented as:

$$\int d^4x e^{-i\hat{q}\cdot x} \langle B | T \{ \Gamma_1(x), \Gamma_2(x) \} | B \rangle = -\frac{1}{m_b} \left[ \langle B | \mathcal{O}_0 | B \rangle + \frac{1}{2m_b} \langle B | \mathcal{O}_1 | B \rangle + \frac{1}{4m_b^2} \langle B | \mathcal{O}_2 | B \rangle + \dots \right], \quad (31)$$

and the expressions for the operators  $\mathcal{O}_0$ ,  $\mathcal{O}_1$  and  $\mathcal{O}_2$  are given explicitly in [33]. They are obtained by expanding the propagators in the Feynman diagrams contributing to the time-ordered product on the l.h.s. of the above equation (see Fig. 1 in [33]), using  $p_{b\mu} = m_b v_\mu + k_\mu$ , fixing the four-velocity of the external  $b$  quark field to be  $v_\mu$  and treating the components of the “residual momentum”  $k_\mu$  to be much smaller than  $m_b$ .

As is well known, the leading power corrections can be parametrized in terms of the matrix elements of the kinetic energy and magnetic moment operators, called  $\lambda_1$  and  $\lambda_2$ , respectively, and defined as,

$$\begin{aligned} \langle B | \bar{h} (i D)^2 h | B \rangle &\equiv 2 M_B \lambda_1, \\ \langle B | \bar{h} \frac{-i}{2} \sigma^{\mu\nu} G_{\mu\nu} h | B \rangle &\equiv 6 M_B \lambda_2, \end{aligned} \quad (32)$$

where  $B$  denotes the pseudoscalar  $B$  meson,  $D_\mu$  is the covariant derivative and  $G_{\mu\nu}$  is the QCD field strength tensor. The two-component effective field in the HQE approach  $h(x)$  is related to the QCD field  $b(x)$  through the expansion,

$$b(x) = e^{im_b v \cdot x} \left[ 1 + i \frac{\mathcal{D}}{2m_b} + \dots \right] h(x), \quad (33)$$

where  $\mathcal{D} = D_\mu \gamma^\mu$ . The parameters  $\lambda_1$  and  $\lambda_2$  are related through the quantity  $\bar{\Lambda}$  to the hadron masses [38],

$$\begin{aligned} m_B &= m_b + \bar{\Lambda} - \frac{\lambda_1 + 3\lambda_2}{2m_b} + \dots, \\ m_{B^*} &= m_b + \bar{\Lambda} - \frac{\lambda_1 - \lambda_2}{2m_b} + \dots. \end{aligned} \quad (34)$$

From the  $B - B^*$  mass difference, one obtains  $\lambda_2 \simeq 0.12$  GeV $^2$ . The quantity  $\lambda_1$  has been determined from QCD sum rules [39, 40] and data [41]. Its present value is subject to a certain

theoretical dispersion, estimated somewhere between  $\lambda_1 = -(0.52 \pm 0.12) \text{ GeV}^2$  (Ball and Braun in [39]) to  $\lambda_1 = -(0.10 \pm 0.05) \text{ GeV}^2$  (Neubert [40]).

Concerning the definitions of the operators in eq. (31), we follow the prescription given in [33], in which the leading operator  $\mathcal{O}_0$  is defined in terms of the “full” four-component field  $b(x)$ ,

$$\mathcal{O}_0(x) = \frac{1}{x} \bar{b} \Gamma_1 (\not{v} - \not{\hat{q}} + \hat{m}_s) \Gamma_2 b, \quad (35)$$

but the other two subleading operators  $\mathcal{O}_1$  and  $\mathcal{O}_2$  are written in terms of the two-component effective fields  $h(x)$ , which is related to the field  $b(x)$  through the expansion given in eq. (33). Of these, the expression for  $\mathcal{O}_2$  involving the expansion of the one-gluon graphs is obtained by a non-trivial derivation, which we have checked, and it agrees with the one given in eq. (3.8) of [33]. (Likewise, we agree with the expression for  $\mathcal{O}_1$  given in eq. (3.6) of [33].)

Using Lorentz decomposition, the tensor  $T_{\mu\nu}$  can be expanded in terms of three structure functions,

$$T_{\mu\nu} = -T_1 g_{\mu\nu} + T_2 v_\mu v_\nu + T_3 i \epsilon_{\mu\nu\alpha\beta} v^\alpha \hat{q}^\beta, \quad (36)$$

where the structure functions which do not contribute to the amplitude in the limit of massless leptons have been neglected. After contracting the hadronic and leptonic tensors, one finds

$$T^{L/R}{}_{\mu\nu} L^{L/R\mu\nu} = m_b^2 \left\{ 2 \hat{s} T_1^{L/R} + \left[ (v \cdot \hat{q})^2 - \frac{1}{4} \hat{u}^2 - \hat{s} \right] T_2^{L/R} \mp \hat{s} \hat{u} T_3^{L/R} \right\}. \quad (37)$$

We remark here that the  $T_3$  term will contribute to the FB asymmetry but not to the branching ratio or the dilepton invariant mass spectrum in the decay  $B \rightarrow X_s \ell^+ \ell^-$ .

The results of the power corrections to the structure functions  $T_i$  can be decomposed into the sum of various terms, denoted by  $T_i^{(j)}$ , which can be traced back to well defined pieces in the evaluation of the time-ordered product given above:

$$T_i(v \cdot \hat{q}, \hat{s}) = \sum_{j=0,1,2,s,g,\delta} T_i^{(j)}(v \cdot \hat{q}, \hat{s}). \quad (38)$$

The expressions for  $T_i^{(j)}(v \cdot \hat{q}, \hat{s})$  calculated up to  $O(M_B/m_b^3)$  are given in Appendix A. They contain the parton model expressions  $T_i^{(0)}(v \cdot \hat{q}, \hat{s})$  and the power correction in the HQE approach which depend on the two HQET-specific parameters  $\lambda_1$  and  $\lambda_2$  defined in eqs. (32). Note that the  $s$ -quark mass terms are explicitly kept in  $T_i^{(j)}(v \cdot \hat{q}, \hat{s})$ .

From the expressions for  $T_i^{(j)}$  given in Appendix A, we see that  $T_i^{(0)}(i = 1, 2, 3)$  are of order  $M_B/(m_b)$  and the rest  $T_i^{(1)}, T_i^{(\delta)}, T_i^{(2)}, T_i^{(s)}$  and  $T_i^{(g)}$  are all of order  $M_B\lambda_1/m_b^3$  or  $M_B\lambda_2/m_b^3$ . Since the ratio  $M_B/m_b = 1 + O(1/m_b)$ , we note that the Dalitz distribution in  $B \rightarrow X_s \ell^+ \ell^-$  has linear corrections in  $1/m_b$ . The origin of the various terms in the expansion given in eq. (38) is as follows:

- The contributions to  $T_i^{(1)}$  come from the matrix element of those terms in the operator  $\mathcal{O}_2$ , which originate from expanding the spinor of the heavy quark field  $b(x)$  in terms of the spinor of the heavy quark effective theory  $h(x)$ .
- The remaining contributions from the matrix element of the operator  $\mathcal{O}_2$  are denoted by  $T_i^{(2)}$  and  $T_i^{(g)}$ , with  $T_i^{(g)}$  originating from the matrix element of the one gluon emission diagram and the rest being  $T_i^{(2)}$ .
- The contributions denoted by  $T_i^{(\delta)}$  arise from the matrix element of the operator  $\mathcal{O}_1$ . In the leading order in  $(1/m_b)$  this matrix element vanishes, but in the sub-leading order it receives a non-trivial contribution which can be calculated by using the equation of motion.
- Finally, the contributions  $T_i^{(s)}$  arise from the matrix element of the scalar operator  $\bar{b}b$ .

Concerning the last point noted above, we recall that the scalar current can be written in terms of the vector current plus higher dimensional operators as [15]

$$\bar{b}b = v_\mu \bar{b} \gamma^\mu b + \frac{1}{2m_b^2} \bar{h} \left[ (iD)^2 - (v \cdot iD)^2 + s^{\mu\nu} G_{\mu\nu} \right] h + \dots, \quad (39)$$

with  $G_{\mu\nu} = [iD_\mu, iD_\nu]$  and  $s^{\mu\nu} = (-i/2)\sigma^{\mu\nu}$ . We note that in deriving  $T_i^{(s)}$ , use has been made of the conservation of the  $b$ -number current in QCD, which yields the normalization:

$$\langle B | \bar{b} \gamma_\mu b | B \rangle = 2(p_B)_\mu. \quad (40)$$

Finally, after doing the integration on the complex plane  $v \cdot \hat{q}$  (see Fig. 1 in [16] for the analytic structure of  $T_{\mu\nu}$  and the contour of integration), we derive the double differential branching ratio in  $B \rightarrow X_s \ell^+ \ell^-$ . The result can be expressed as,

$$\frac{d\mathcal{B}}{d\hat{s} d\hat{u}} = \mathcal{B}_0 \left( \left\{ \left[ (1 - \hat{m}_s^2)^2 - \hat{s}^2 - \hat{u}^2 - \frac{1}{3} (2 \hat{\lambda}_1 (-1 + 2\hat{m}_s^2 - \hat{m}_s^4) - 2\hat{s} + \hat{s}^2) \right. \right. \right.$$

$$\begin{aligned}
& + 3 \hat{\lambda}_2 (-1 + 6\hat{m}_s^2 - 5\hat{m}_s^4 - 8\hat{s} + 5\hat{s}^2) \Big] \left( |C_9^{\text{eff}}|^2 + |C_{10}|^2 \right) \\
& + \left[ 4 \left( 1 - \hat{m}_s^2 - \hat{m}_s^4 + \hat{m}_s^6 - 8\hat{m}_s^2\hat{s} - \hat{s}^2 - \hat{m}_s^2\hat{s}^2 + \hat{u}^2 + \hat{m}_s^2\hat{u}^2 \right) \right. \\
& \left. - \frac{4}{3} \left( 2\hat{\lambda}_1 (-1 + \hat{m}_s^2 + \hat{m}_s^4 - \hat{m}_s^6 + 2\hat{s} + 10\hat{m}_s^2\hat{s} + \hat{s}^2 + \hat{m}_s^2\hat{s}^2) \right. \right. \\
& \left. \left. + 3\hat{\lambda}_2 (3 + 5\hat{m}_s^2 - 3\hat{m}_s^4 - 5\hat{m}_s^6 + 4\hat{s} + 28\hat{m}_s^2\hat{s} + 5\hat{s}^2 + 5\hat{m}_s^2\hat{s}^2) \right) \right] \frac{|C_7^{\text{eff}}|^2}{\hat{s}} \\
& - 8 \left[ (\hat{s}(1 + \hat{m}_s^2) - (1 - \hat{m}_s^2)^2) + \frac{2}{3}\hat{\lambda}_1 (-1 + 2\hat{m}_s^2 - \hat{m}_s^4 + \hat{s} + \hat{m}_s^2\hat{s}) \right. \\
& \left. + \hat{\lambda}_2 (5\hat{m}_s^2 - 5\hat{m}_s^4 + 2\hat{s} + 5\hat{m}_s^2\hat{s}) \right] \text{Re}(C_9^{\text{eff}}) C_7^{\text{eff}} \\
& + 2 \left[ 2 + \hat{\lambda}_1 + 5\hat{\lambda}_2 \right] \hat{u}\hat{s} \text{Re}(C_9^{\text{eff}}) C_{10} \\
& + 4 \left[ 2 \left( 1 + \hat{m}_s^2 \right) + \hat{\lambda}_1 (1 + \hat{m}_s^2) + \hat{\lambda}_2 (3 + 5\hat{m}_s^2) \right] \hat{u} \text{Re}(C_{10}) C_7^{\text{eff}} \Big\} \theta \left[ \hat{u}(\hat{s}, \hat{m}_s)^2 - \hat{u}^2 \right] \\
& - E_1(\hat{s}, \hat{u}) \delta \left[ \hat{u}(\hat{s}, \hat{m}_s)^2 - \hat{u}^2 \right] - E_2(\hat{s}, \hat{u}) \delta' \left[ \hat{u}(\hat{s}, \hat{m}_s)^2 - \hat{u}^2 \right]. \quad (41)
\end{aligned}$$

The auxiliary functions  $E_i(\hat{s}, \hat{u})$  ( $i = 1, 2$ ), introduced here for ease of writing, are given explicitly in Appendix B. The boundary of the Dalitz distribution is as usual determined by the argument of the  $\theta$ -function and in the  $(\hat{u}, \hat{s})$ -plane it has been specified earlier. The analytic form of the result (41) is very similar to the corresponding double differential distributions derived by Manohar and Wise in [16] for the semileptonic decays  $B \rightarrow (X_c, X_u)\ell\nu_\ell$ . Further comparisons with this work in the  $V - A$  limit for the single differential and integrated rates are given in Appendix C.

It has become customary to express the branching ratio for  $B \rightarrow X_s\ell^+\ell^-$  in terms of the well-measured semileptonic branching ratio  $\mathcal{B}_{sl}$  for the decays  $B \rightarrow (X_c, X_u)\ell\nu_\ell$ . This fixes the normalization constant  $\mathcal{B}_0$  to be,

$$\mathcal{B}_0 \equiv \mathcal{B}_{sl} \frac{3\alpha^2}{16\pi^2} \frac{|V_{ts}^* V_{tb}|^2}{|V_{cb}|^2} \frac{1}{f(\hat{m}_c)\kappa(\hat{m}_c)}, \quad (42)$$

where

$$f(\hat{m}_c) = 1 - 8\hat{m}_c^2 + 8\hat{m}_c^6 - \hat{m}_c^8 - 24\hat{m}_c^4 \ln \hat{m}_c \quad (43)$$

is the phase space function for  $\Gamma(B \rightarrow X_c l\nu)$  in the lowest order (i.e., parton model) and the function  $\kappa(\hat{m}_c)$  accounts for both the  $O(\alpha_s)$  QCD correction to the semi-leptonic decay width [22, 37] and the leading order  $(1/m_b)^2$  power correction [15]. Written explicitly, it reads as:

$$\kappa(\hat{m}_c) = 1 - \frac{2\alpha_s(m_b)}{3\pi} g(\hat{m}_c) + \frac{h(\hat{m}_c)}{2m_b^2}, \quad (44)$$

where the two functions are:

$$\begin{aligned} g(\hat{m}_c) &= (\pi^2 - \frac{31}{4})(1 - \hat{m}_c)^2 + \frac{3}{2}, \\ h(\hat{m}_c) &= \lambda_1 + \frac{\lambda_2}{f(\hat{m}_c)} \left[ -9 + 24\hat{m}_c^2 - 72\hat{m}_c^4 + 72\hat{m}_c^6 - 15\hat{m}_c^8 - 72\hat{m}_c^4 \ln \hat{m}_c \right]. \end{aligned} \quad (45)$$

Finally, after integrating over the variable  $\hat{u}$ , we derive the differential branching ratio in the scaled dilepton invariant mass for  $B \rightarrow X_s \ell^+ \ell^-$ ,

$$\begin{aligned} \frac{d\mathcal{B}}{d\hat{s}} &= 2 \mathcal{B}_0 \left\{ \left[ \frac{2}{3} \hat{u}(\hat{s}, \hat{m}_s) ((1 - \hat{m}_s^2)^2 + \hat{s}(1 + \hat{m}_s^2) - 2\hat{s}^2) + \frac{1}{3} (1 - 4\hat{m}_s^2 + 6\hat{m}_s^4 - 4\hat{m}_s^6 + \hat{m}_s^8 - \hat{s} \right. \right. \\ &\quad + \hat{m}_s^2 \hat{s} + \hat{m}_s^4 \hat{s} - \hat{m}_s^6 \hat{s} - 3\hat{s}^2 - 2\hat{m}_s^2 \hat{s}^2 - 3\hat{m}_s^4 \hat{s}^2 + 5\hat{s}^3 + 5\hat{m}_s^2 \hat{s}^3 - 2\hat{s}^4) \frac{\hat{\lambda}_1}{\hat{u}(\hat{s}, \hat{m}_s)} \\ &\quad + (1 - 8\hat{m}_s^2 + 18\hat{m}_s^4 - 16\hat{m}_s^6 + 5\hat{m}_s^8 - \hat{s} - 3\hat{m}_s^2 \hat{s} + 9\hat{m}_s^4 \hat{s} - 5\hat{m}_s^6 \hat{s} - 15\hat{s}^2 - 18\hat{m}_s^2 \hat{s}^2 \\ &\quad - 15\hat{m}_s^4 \hat{s}^2 + 25\hat{s}^3 + 25\hat{m}_s^2 \hat{s}^3 - 10\hat{s}^4) \frac{\hat{\lambda}_2}{\hat{u}(\hat{s}, \hat{m}_s)} \left. \right] \left( |C_9^{\text{eff}}|^2 + |C_{10}|^2 \right) \\ &\quad + \left[ \frac{8}{3} \hat{u}(\hat{s}, \hat{m}_s) (2(1 + \hat{m}_s^2)(1 - \hat{m}_s^2)^2 - (1 + 14\hat{m}_s^2 + \hat{m}_s^4) \hat{s} - (1 + \hat{m}_s^2) \hat{s}^2) \right. \\ &\quad + \frac{4}{3} (2 - 6\hat{m}_s^2 + 4\hat{m}_s^4 + 4\hat{m}_s^6 - 6\hat{m}_s^8 + 2\hat{m}_s^{10} - 5\hat{s} - 12\hat{m}_s^2 \hat{s} + 34\hat{m}_s^4 \hat{s} - 12\hat{m}_s^6 \hat{s} - 5\hat{m}_s^8 \hat{s} + 3\hat{s}^2 \\ &\quad + 29\hat{m}_s^2 \hat{s}^2 + 29\hat{m}_s^4 \hat{s}^2 + 3\hat{m}_s^6 \hat{s}^2 + \hat{s}^3 - 10\hat{m}_s^2 \hat{s}^3 + \hat{m}_s^4 \hat{s}^3 - \hat{s}^4 - \hat{m}_s^2 \hat{s}^4) \frac{\hat{\lambda}_1}{\hat{u}(\hat{s}, \hat{m}_s)} + 4 (-6 + 2\hat{m}_s^2 \\ &\quad + 20\hat{m}_s^4 - 12\hat{m}_s^6 - 14\hat{m}_s^8 + 10\hat{m}_s^{10} + 3\hat{s} + 16\hat{m}_s^2 \hat{s} + 62\hat{m}_s^4 \hat{s} - 56\hat{m}_s^6 \hat{s} - 25\hat{m}_s^8 \hat{s} + 3\hat{s}^2 \\ &\quad + 73\hat{m}_s^2 \hat{s}^2 + 101\hat{m}_s^4 \hat{s}^2 + 15\hat{m}_s^6 \hat{s}^2 + 5\hat{s}^3 - 26\hat{m}_s^2 \hat{s}^3 + 5\hat{m}_s^4 \hat{s}^3 - 5\hat{s}^4 - 5\hat{m}_s^2 \hat{s}^4) \frac{\hat{\lambda}_2}{\hat{u}(\hat{s}, \hat{m}_s)} \left. \right] \frac{|C_7^{\text{eff}}|^2}{\hat{s}} \\ &\quad + \left[ 8\hat{u}(\hat{s}, \hat{m}_s) ((1 - \hat{m}_s^2)^2 - (1 + \hat{m}_s^2) \hat{s}) + 4(1 - 2\hat{m}_s^2 + \hat{m}_s^4 - \hat{s} - \hat{m}_s^2 \hat{s}) \hat{u}(\hat{s}, \hat{m}_s) \hat{\lambda}_1 \right. \\ &\quad + 4 (-5 + 30\hat{m}_s^4 - 40\hat{m}_s^6 + 15\hat{m}_s^8 - \hat{s} + 21\hat{m}_s^2 \hat{s} + 25\hat{m}_s^4 \hat{s} - 45\hat{m}_s^6 \hat{s} + 13\hat{s}^2 + 22\hat{m}_s^2 \hat{s}^2 \\ &\quad \left. + 45\hat{m}_s^4 \hat{s}^2 - 7\hat{s}^3 - 15\hat{m}_s^2 \hat{s}^3) \frac{\hat{\lambda}_2}{\hat{u}(\hat{s}, \hat{m}_s)} \right] \text{Re}(C_9^{\text{eff}}) C_7^{\text{eff}} \Big\}. \end{aligned} \quad (46)$$

Another interesting quantity is the FB asymmetry defined in [34, 35]

$$\frac{d\mathcal{A}(\hat{s})}{d\hat{s}} = \int_0^1 \frac{d^2\mathcal{B}}{d\hat{s} dz} dz - \int_{-1}^0 \frac{d^2\mathcal{B}}{d\hat{s} dz} dz, \quad (47)$$

where  $z \equiv \cos \theta$  is the angle of  $\ell^+$  measured w.r.t. the  $b$ -quark direction in the dilepton c.m. system. The leading power corrected expression for the FB-asymmetry  $\mathcal{A}(\hat{s})$  is:

$$\begin{aligned} \frac{d\mathcal{A}(\hat{s})}{d\hat{s}} &= -2 \mathcal{B}_0 \left\{ \left[ 2(\hat{u}(\hat{s}, \hat{m}_s))^2 \hat{s} + \frac{\hat{s}}{3} (3 - 6\hat{m}_s^2 + 3\hat{m}_s^4 + 2\hat{s} - 6\hat{m}_s^2 \hat{s} + 3\hat{s}^2) \hat{\lambda}_1 \right. \right. \\ &\quad \left. \left. + \hat{s} (-9 - 6\hat{m}_s^2 + 15\hat{m}_s^4 - 14\hat{s} - 30\hat{m}_s^2 \hat{s} + 15\hat{s}^2) \hat{\lambda}_2 \right] \text{Re}(C_9^{\text{eff}}) C_{10} \right\} \end{aligned}$$

$$\begin{aligned}
& + \left[ 4(\hat{u}(\hat{s}, \hat{m}_s))^2 (1 + \hat{m}_s^2) + \frac{2}{3} (1 + \hat{m}_s^2) (3 - 6\hat{m}_s^2 + 3\hat{m}_s^4 + 2\hat{s} - 6\hat{m}_s^2\hat{s} + 3\hat{s}^2) \hat{\lambda}_1 \right. \\
& \left. + 2(-7 - 3\hat{m}_s^2 - 5\hat{m}_s^4 + 15\hat{m}_s^6 - 10\hat{s} - 24\hat{m}_s^2\hat{s} - 30\hat{m}_s^4\hat{s} + 9\hat{s}^2 + 15\hat{m}_s^2\hat{s}^2) \hat{\lambda}_2 \right] \text{Re}(C_{10}) C_7^{\text{eff}} \} . \\
\end{aligned} \tag{48}$$

From the experimental point of view, a more useful quantity is the normalized FB-asymmetry, obtained by normalizing  $d\mathcal{A}/d\hat{s}$  with the dilepton mass distribution,  $d\mathcal{B}/d\hat{s}$ ,

$$\frac{d\bar{\mathcal{A}}}{d\hat{s}} = \frac{d\mathcal{A}}{d\hat{s}} / \frac{d\mathcal{B}}{d\hat{s}} . \tag{49}$$

This asymmetry, which we recall is defined in the dilepton c.m.s. frame, is identical to the energy asymmetry introduced in [36], which is defined in the  $B$  rest frame, as shown in Appendix D.

The results derived for the  $O(\alpha_s)$ -improved and power-corrected Dalitz distribution, dilepton invariant mass, and FB-asymmetry in  $B \rightarrow X_s \ell^+ \ell^-$  are the principal new results in this section. It is useful to write the corresponding expressions in the limit  $m_s = 0$ . For the dilepton invariant mass distribution, we get

$$\begin{aligned}
\frac{d\mathcal{B}}{d\hat{s}} = & 2 \mathcal{B}_0 \left\{ \left[ \frac{1}{3} (1 - \hat{s})^2 (1 + 2\hat{s}) (2 + \hat{\lambda}_1) + (1 - 15\hat{s}^2 + 10\hat{s}^3) \hat{\lambda}_2 \right] \left( |C_9^{\text{eff}}|^2 + |C_{10}|^2 \right) \right. \\
& + \left[ \frac{4}{3} (1 - \hat{s})^2 (2 + \hat{s}) (2 + \hat{\lambda}_1) + 4 (-6 - 3\hat{s} + 5\hat{s}^3) \hat{\lambda}_2 \right] \frac{|C_7^{\text{eff}}|^2}{\hat{s}} \\
& \left. + \left[ 4(1 - \hat{s})^2 (2 + \hat{\lambda}_1) + 4 (-5 - 6\hat{s} + 7\hat{s}^2) \hat{\lambda}_2 \right] \text{Re}(C_9^{\text{eff}}) C_7^{\text{eff}} \right\} . \\
\end{aligned} \tag{50}$$

The (unnormalized) FB asymmetry reads as,

$$\begin{aligned}
\frac{d\mathcal{A}}{d\hat{s}} = & -2 \mathcal{B}_0 \left\{ \left[ 2(1 - \hat{s})^2 \hat{s} + \frac{\hat{s}}{3} (3 + 2\hat{s} + 3\hat{s}^2) \hat{\lambda}_1 + \hat{s} (-9 - 14\hat{s} + 15\hat{s}^2) \hat{\lambda}_2 \right] \text{Re}(C_9^{\text{eff}}) C_{10} \right. \\
& \left. + \left[ 4(1 - \hat{s})^2 + \frac{2}{3} (3 + 2\hat{s} + 3\hat{s}^2) \hat{\lambda}_1 + 2(-7 - 10\hat{s} + 9\hat{s}^2) \hat{\lambda}_2 \right] \text{Re}(C_{10}) C_7^{\text{eff}} \right\} . \\
\end{aligned} \tag{51}$$

A direct comparison of our result for the dilepton invariant mass distribution given in eq. (50) above can now be made with the differential decay width  $d\Gamma(B \rightarrow X_s \ell^+ \ell^-)/d\hat{s}$  derived in eq. (3.21) of the paper by FLS [33]. To that end, one has to take into account the (obvious) normalization difference between the decay width and branching ratio, rewrite the quantities  $A^i$  and  $B^i$  used in FLS [33] in terms of the Wilson coefficients,  $C_7^{\text{eff}}$ ,  $C_9^{\text{eff}}$  and  $C_{10}$  used by us, and drop the explicit  $O(\alpha_s)$ -improvement in the coefficient  $C_9^{\text{eff}}$ , as FLS did not include it in their calculations. We leave this as an instructive exercise for the interested reader and go on to make the following comparative observations:

- The results derived here and in FLS [33] reproduce the known parton model expression for the dilepton invariant mass distribution in the limit  $\lambda_1 \rightarrow 0$  and  $\lambda_2 \rightarrow 0$ .
- The power corrections themselves, i.e. the expressions multiplying the constants  $\lambda_1$  and  $\lambda_2$ , are *different* in the two derivations.
- The power-corrected dilepton invariant mass distribution derived by us retains the characteristic  $1/\hat{s}$  behaviour following from the one-photon exchange in the parton model, in contradiction to the observations made in [33].
- Leading order power corrections in the dilepton mass distribution are found to be small over a good part of the dilepton mass  $\hat{s}$ . However, we find that the power corrections become increasingly large and negative as one approaches  $\hat{s} \rightarrow \hat{s}^{max}$ . Since the parton model spectrum falls steeply near the end-point  $\hat{s} \rightarrow \hat{s}^{max}$ , this leads to the uncomfortable result that the power corrected dilepton mass distribution becomes negative for the high dilepton masses - in contradiction to the observations made in [33]. We show in Fig. 1 this distribution in the parton model and the HQE approach, using the central values of the parameters in Table 1.
- We note that the correction proportional to the kinetic energy term  $\hat{\lambda}_1$  renormalizes the parton model invariant mass distribution multiplicatively by the factor  $(1 + \lambda_1/(2m_b^2))$ , i.e. no new functional dependence in  $\hat{s}$  is introduced (moreover, this factor is hardly different from 1). Hence, the negative probability near the end-point is largely driven by the magnetic moment term  $\hat{\lambda}_2$ .
- A comparison of the dilepton mass spectrum resulting from eq. (50) of this work and eq. (3.21) in FLS [33] is shown in Fig. 2, where we have used the input parameters given in Table 1, except that we have set  $m_s = 0$  to conform to the FLS derivation. The two curves differ in the large  $\hat{s}$  region with ours becoming negative before the kinematic end-point is actually reached.

The normalized FB asymmetry,  $d\bar{A}(\hat{s})/d\hat{s}$ , in the HQE-approach and the parton model are shown in Fig. 3. We find that this asymmetry is stable against leading order power corrections up to  $\hat{s} \leq 0.6$ , but the corrections become increasingly large and eventually uncontrollable

due to the unphysical behaviour of the HQE-based dilepton mass distribution as  $\hat{s}$  approaches  $\hat{s}^{max}$  (see Fig. 2). Based on these investigations (and, of course, barring an error on our part!), we must conclude that the HQE-based approach has a restrictive kinematical domain for its validity. In particular, it breaks down for the high dilepton invariant mass region in  $B \rightarrow X_s \ell^+ \ell^-$ .

Parameter	Value
$m_W$	80.26 (GeV)
$m_Z$	91.19 (GeV)
$\sin^2 \theta_W$	0.2325
$m_s$	0.2 (GeV)
$m_c$	1.4 (GeV)
$m_b$	4.8 (GeV)
$m_t$	$175 \pm 9$ (GeV)
$\mu$	$5_{-2.5}^{+5.0}$ (GeV)
$\Lambda_{QCD}^{(5)}$	$0.214_{-0.054}^{+0.066}$ (GeV)
$\alpha_{QED}^{-1}$	129
$\alpha_s(m_Z)$	$0.117 \pm 0.005$
$\mathcal{B}_{sl}$	$(10.4 \pm 0.4)$ %
$\lambda_1$	$-0.20$ (GeV $^2$ )
$\lambda_2$	$+0.12$ (GeV $^2$ )

Table 1: Values of the input parameters used in the numerical calculations of decay rates. Unless, otherwise specified, we use the central values.

Coefficient	Value
$C^{(0)}$	+0.3805
$C_{\text{eff}}^7$	-0.3110
$C_9^{NDR}$	+4.1530
$C_{10}$	-4.5461

Table 2: Wilson coefficients used in the numerical calculations corresponding to the central values given in Table 1.

This behaviour of the dilepton mass spectrum in  $B \rightarrow X_s \ell^+ \ell^-$  is not unexpected, as similar behaviours have been derived near the end-point of the lepton energy spectra in the decays  $B \rightarrow X \ell \nu_\ell$  in the HQE approach [16]. To stress these similarities, we show the power correction in the dilepton mass distribution as calculated in the HQE approach compared to the parton

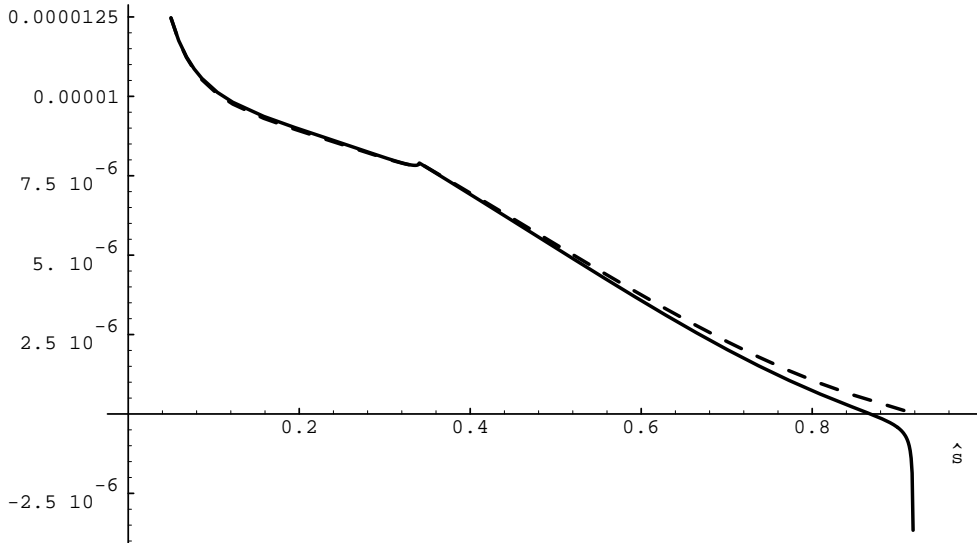


Figure 1: Dilepton invariant mass spectrum  $d\mathcal{B}(B \rightarrow X_s e^+ e^-)/d\hat{s}$  in the parton model (dashed curve) and with leading power corrections calculated in the HQE approach (solid curve). The parameters used are given in Table 1.

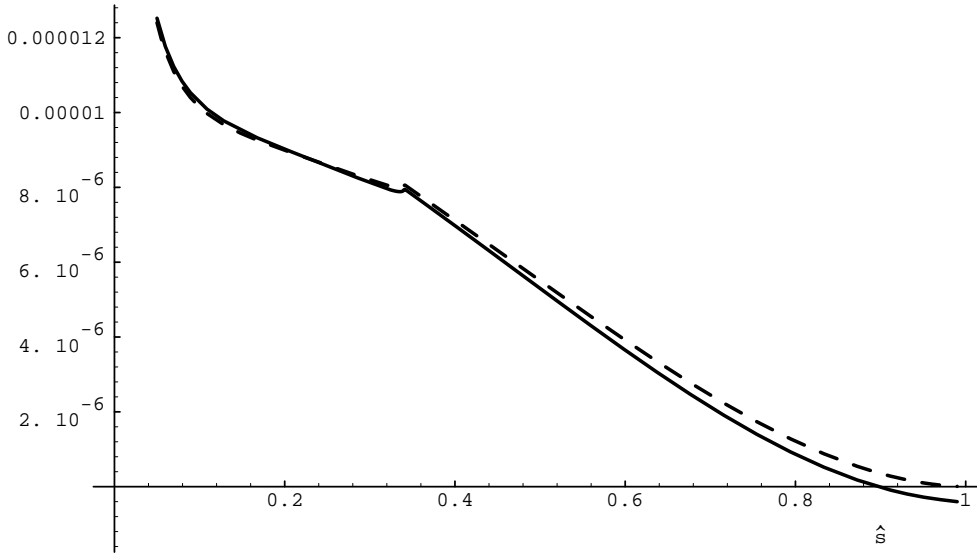


Figure 2: Dilepton invariant mass spectrum  $d\mathcal{B}(B \rightarrow X_s e^+ e^-)/d\hat{s}$  with power corrections calculated in the HQE approach. The solid curve corresponds to our calculation and the dashed curve results from eq. (3.21) of FLS [33] with  $m_s = 0$ . The other parameters are given in Table 1.

model through the ratio defined as:

$$R^{\text{HQE}}(\hat{s}) \equiv \frac{d\mathcal{B}/d\hat{s}(\text{HQE}) - d\mathcal{B}/d\hat{s}(\text{Parton Model})}{d\mathcal{B}/d\hat{s}(\text{Parton Model})} \quad (52)$$

The correction factor  $R^{\text{HQE}}(\hat{s})$  for  $B \rightarrow X_s \ell^+ \ell^-$  shown in Fig. 4 is qualitatively similar to the corresponding factor in the lepton energy spectrum in the decay  $B \rightarrow X_c \ell \nu_\ell$ , given in Fig.

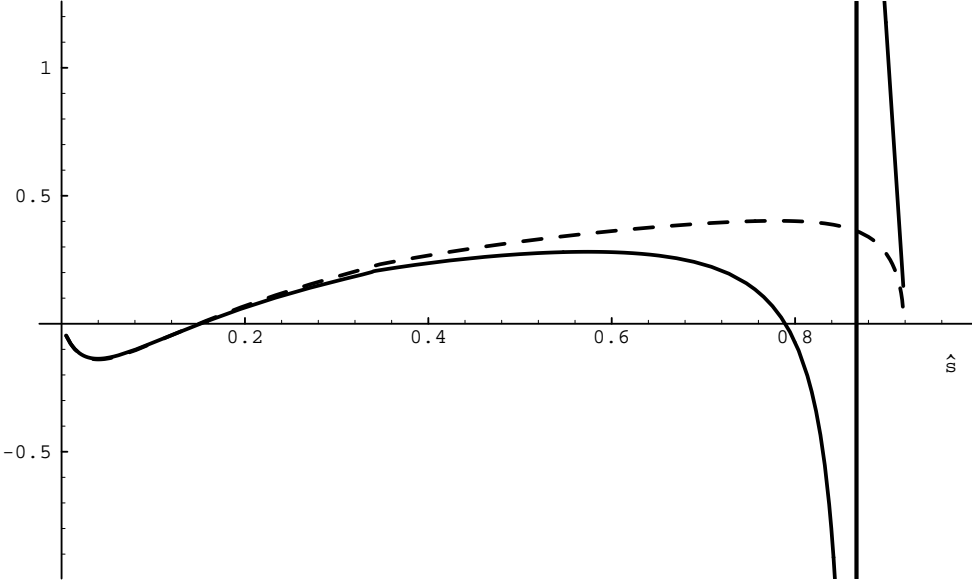


Figure 3: FB asymmetry (normalized)  $d\bar{\mathcal{A}}(B \rightarrow X_s e^+ e^-)/d\hat{s}$  in the parton model and with power corrections calculated in the HQE approach. The solid curve corresponds to the HQE spectrum and the dashed curve is the parton model result. The parameters used are given in Table 1.

6 of [16]. Finally, we note that we have been able to derive the power corrected rate for the semileptonic decays  $B \rightarrow X_c \ell \nu_\ell$  obtained by Manohar and Wise in [16], taking the appropriate limits of our calculations and taking into account the differences in our normalization of states and conventions, as shown in Appendix C.

Finally, since the HQE-improved expression for the decay rate including the  $s$ -quark mass effects is rather long, we give below the results in a numerical form:

$$\Gamma^{\text{HQE}} = \Gamma^b(1 + C_1 \hat{\lambda}_1 + C_2 \hat{\lambda}_2), \quad (53)$$

where  $\Gamma^b$  is the parton model decay width for  $b \rightarrow s \ell^+ \ell^-$  and the coefficients depend on the input parameters. For the central values of the parameters given in Table 1, they have the values  $C_1 = 0.501$  and  $C_2 = -7.425$ . This leads to a reduction in the decay width by  $-4.1\%$ , using the values of  $\lambda_1$  and  $\lambda_2$  given in Table 1. Moreover, this reduction is mostly contributed by the  $\lambda_2$ -dependent term. We recall that the coefficient of the  $\hat{\lambda}_1$  term above is the same as in the semileptonic width  $\Gamma(B \rightarrow X_u \ell \nu_\ell)$ , but the coefficient of the  $\hat{\lambda}_2$  term above is larger than the corresponding coefficient ( $= -9/2$ ) in the semileptonic decay width. Hence, the power corrections in  $\Gamma(B \rightarrow X_u \ell \nu_\ell)$  and  $\Gamma(B \rightarrow X_s \ell^+ \ell^-)$  are rather similar but not identical.

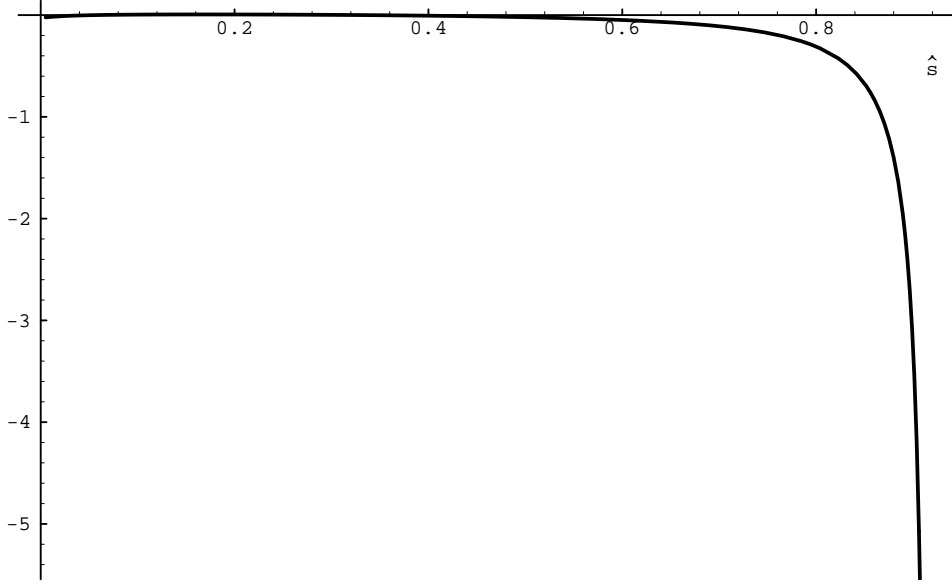


Figure 4: The correction factor  $R^{HQE}(s)$  (in percentage) as defined in eq. (52) for the dilepton mass spectrum  $d\mathcal{B}(B \rightarrow X_s \ell^+ \ell^-)/d\hat{s}$ . The parameters used are given in Table 1.

### 3 $B$ -meson Wave function Effects in $B \rightarrow X_s \ell^+ \ell^-$

In this section, we present our estimates of the non-perturbative effects on the decay distributions in  $B \rightarrow X_s \ell^+ \ell^-$ . These effects are connected with the bound state nature of the  $B$  hadron and the physical threshold in the  $B \rightarrow X_s \ell^+ \ell^-$  in the final state. In order to implement these effects on the decay distributions in  $B \rightarrow X_s \ell^+ \ell^-$ , we resort to the Gaussian Fermi motion model introduced in [22]. In this model, the  $B$ -meson consists of a  $b$ -quark and an spectator antiquark  $\bar{q}$  and the four-momenta of the constituents are required to add up to the four-momentum of the  $B$ -meson. In the rest frame of the  $B$ -meson the  $b$ -quark and the spectator move back-to-back with three momenta  $\vec{p}_b = -\vec{p}_q \equiv \vec{p}$ . Energy conservation then implies the equation

$$m_B = \sqrt{m_b^2 + \vec{p}^2} + \sqrt{m_q^2 + \vec{p}^2} \quad ,$$

which can only hold for all values of  $|\vec{p}|$ , if at least one of the masses becomes momentum dependent. We treat the spectator quark  $m_q$  as a momentum-independent parameter; the  $b$ -quark mass is then momentum dependent and we denote it by  $W(p)$ :

$$W^2(p) = M_B^2 + m_q^2 - 2M_B \sqrt{p^2 + m_q^2} \quad . \quad (54)$$

The  $b$ -quark, whose decays determine the dynamics, is given a non-zero momentum having a Gaussian distribution, with the width determined by the parameter  $p_F$ :

$$\phi(p) = \frac{4}{\sqrt{\pi} p_F^3} \exp\left(\frac{-p^2}{p_F^2}\right) \quad ; \quad p = |\vec{p}| , \quad (55)$$

with the normalization  $\int_0^\infty dp p^2 \phi(p) = 1$ . The distributions from the decay of the  $B$ -meson at rest are then obtained by convoluting the appropriately boosted partonic distributions with the Gaussian distribution. The resulting spectra and decay rates depend essentially on two parameters,  $p_F$ , determining the non-perturbative width of the momentum distribution, and  $m_q$  (or equivalently  $W(p)$ ), which determines the height. In the Fermi motion model, the problem of negative probabilities encountered in the HQE approach for the high dilepton masses near  $s \rightarrow s_{max}$  is not present, which motivates us to use this model as a reasonable approximation of the non-perturbative effects in the entire dilepton mass range. The success of this model in describing the inclusive lepton energy spectra in  $B \rightarrow (X_c, X_u)\ell\nu_\ell$  and  $B \rightarrow X_s\gamma$  strengthens this hope.

In the decay  $B \rightarrow X_s\ell^+\ell^-$ , the distribution  $d\mathcal{B}/d\hat{s}$  depends on the Lorentz-invariant variable  $\hat{s}$  only. So, the Lorentz boost involved in the Fermi motion model (Doppler shift) leaves the dilepton mass distribution invariant. However, since the  $b$ -quark mass  $W(p)$  is now a momentum-dependent quantity, this distribution is affected due to the difference  $(W(p) - m_b)$  (mass defect), which rescales the variable  $\hat{s}$  and hence smears the dilepton distribution calculated in the parton model. For different choices of the model parameters  $(p_F, m_q)$  corresponding to the same effective  $b$ -quark mass,  $\langle W \rangle$ , the dilepton mass distributions should be very similar [24], which indeed is the case as we have checked numerically but do not show the resulting distributions here.

The situation with the FB asymmetry (or the energy asymmetry) is, however, quite different. Being an angular-dependent quantity, it is not Lorentz-invariant and is sensitive to both the Doppler shift and the mass defect. We give in Appendix E, the Dalitz distribution  $d^2\Gamma(B \rightarrow X_s\ell^+\ell^-)/dsdu$  in the Fermi motion model, given the partonic double distribution  $d^2\Gamma(b \rightarrow s\ell^+\ell^-)/d\hat{s}d\hat{u}$  in the  $b$ -quark rest frame. These details, hopefully, will be useful in the analysis of data in  $B \rightarrow X_s\ell^+\ell^-$  due to the popularity of the Fermi motion model.

As we calculate the branching ratio for the inclusive decay  $B \rightarrow X_s\ell^+\ell^-$  in terms of the semileptonic decay branching ratio  $\mathcal{B}(B \rightarrow X\ell\nu_\ell)$ , we have to correct the normalization due

to the variable  $b$ -quark mass in both the decay rates. To get the decay rates in this model one first implements the wave function effects and then integrates the spectra. Fixing  $m_b$  but varying the model parameters  $p_F$  and  $m_q$  yields variable effective (momentum-dependent)  $b$ -quark mass  $\langle W \rangle$ . We recall that the decay widths for  $B \rightarrow X_s \ell^+ \ell^-$  and  $B \rightarrow X \ell \nu_\ell$  in this model are proportional to  $\langle W^5 \rangle$  [8]. Hence the decay widths for both the decays individually are rather sensitive to  $\langle W \rangle$ . This dependence largely (but not exactly) cancels out in the branching ratio  $\mathcal{B}(B \rightarrow X_s \ell^+ \ell^-)$ . Thus, varying  $\langle W \rangle$  in the range  $\langle W \rangle = 4.8 \pm 0.1$  GeV results in  $\Delta \Gamma(B \rightarrow X_s \ell^+ \ell^-)/\Gamma = \pm 10.8\%$ . However, the change in the branching ratio itself is rather modest, namely  $\Delta \mathcal{B}(B \rightarrow X_s \ell^+ \ell^-)/\mathcal{B} = \pm 2.3\%$ . This is rather similar to what we have obtained in the HQE approach.

The theoretical uncertainties in the branching ratios for  $B \rightarrow X_s \ell^+ \ell^-$  from the perturbative part, such as the ones from the indeterminacy in the top quark mass, the QCD scale  $\Lambda_{QCD}$  and the renormalization scale  $\mu$ , have been investigated in the literature [27, 28]. We have recalculated them for the indicated ranges of the parameters in Table 1. The resulting (SD) branching ratios and their present uncertainties are found to be:

$$\begin{aligned} \mathcal{B}(B \rightarrow X_s e^+ e^-) &= (8.4 \pm 2.3) \times 10^{-6}, \\ \mathcal{B}(B \rightarrow X_s \mu^+ \mu^-) &= (5.7 \pm 1.2) \times 10^{-6}, \\ \mathcal{B}(B \rightarrow X_s \tau^+ \tau^-) &= (2.6 \pm 0.5) \times 10^{-7}, \end{aligned} \quad (56)$$

where in calculating the branching ratio  $\mathcal{B}(B \rightarrow X_s \tau^+ \tau^-)$ , we have included the  $\tau$ -lepton mass terms in the matrix element [31]. These uncertainties, typically  $\pm 25\%$ , are much larger than the wave-function-dependent uncertainties, and so the theoretical accuracy of the SD-part in the SM in these decays is not compromised by the non-perturbative effects.

We show the resulting dilepton invariant mass distribution in Fig. 5 and the FB-asymmetry in Fig. 6, where for the sake of illustration we have used the values  $(p_F, m_q) = (252, 300)$  (both in MeV), which correspond to an allowed set of parameters obtained from the analysis of the measured photon energy spectrum in  $B \rightarrow X_s \gamma$ , using the same model [9]. We see that the dilepton mass distribution is very stable against Fermi motion effects over most part of this spectrum, as expected. The end-point spectrum in this model extends to the physical kinematic limit in  $B \rightarrow X_s \ell^+ \ell^-$ ,  $s^{max} = (m_B - m_K)^2$ , which obtains for  $m(X_s) = m_K$ , as opposed to the parton model, in which  $s^{max} = (m_b - m_s)^2$ . The two thresholds can be made to coincide

for only unrealistically high values of  $m_b$  and  $m_s$ . The FB-asymmetry shows a more marked dependence on the model parameters, which becomes very significant in the high dilepton mass region.

As the parameters of the Fermi motion model are not presently very well-determined from the fits of the existing data [9, 23], one has to vary these parameters and estimate the resulting dispersion on the distributions in  $B \rightarrow X_s \ell^+ \ell^-$ . We show in Figs. 7 and 8 the dilepton mass distribution and the FB asymmetry, respectively, indicating also the ranges of the parameters  $(p_F, m_q)$ . The resulting theoretical uncertainty in the distributions is found to be modest.

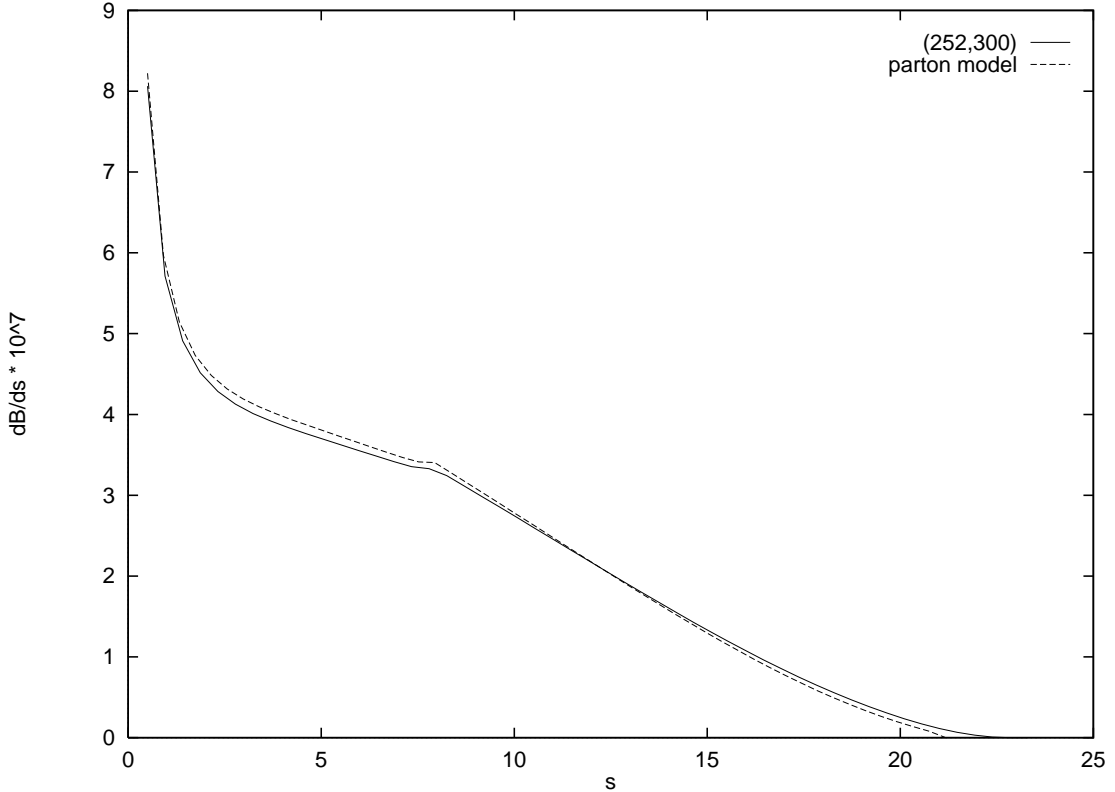


Figure 5: Differential branching ratio  $d\mathcal{B}/ds$  for  $B \rightarrow X_s \ell^+ \ell^-$  in the SM including the next-to-leading order QCD corrections. The dashed curve corresponds to the parton model with the parameters given in Table 1 and the solid curve results from the Fermi motion model with the model parameters  $(p_F, m_q) = (252, 300)$  MeV, yielding an effective  $b$ -quark mass  $\langle W \rangle = 4.85$  GeV.

## 4 LD contributions in $B \rightarrow X_s \ell^+ \ell^-$

Next, we implement the effects of LD contributions in the processes  $B \rightarrow X_s \ell^+ \ell^-$ . The issues involved here have been discussed recently in [30]-[32] and so we will be short in this part. The LD contributions due to the vector mesons  $J/\psi$  and  $\psi'$  and higher resonances, as well as the

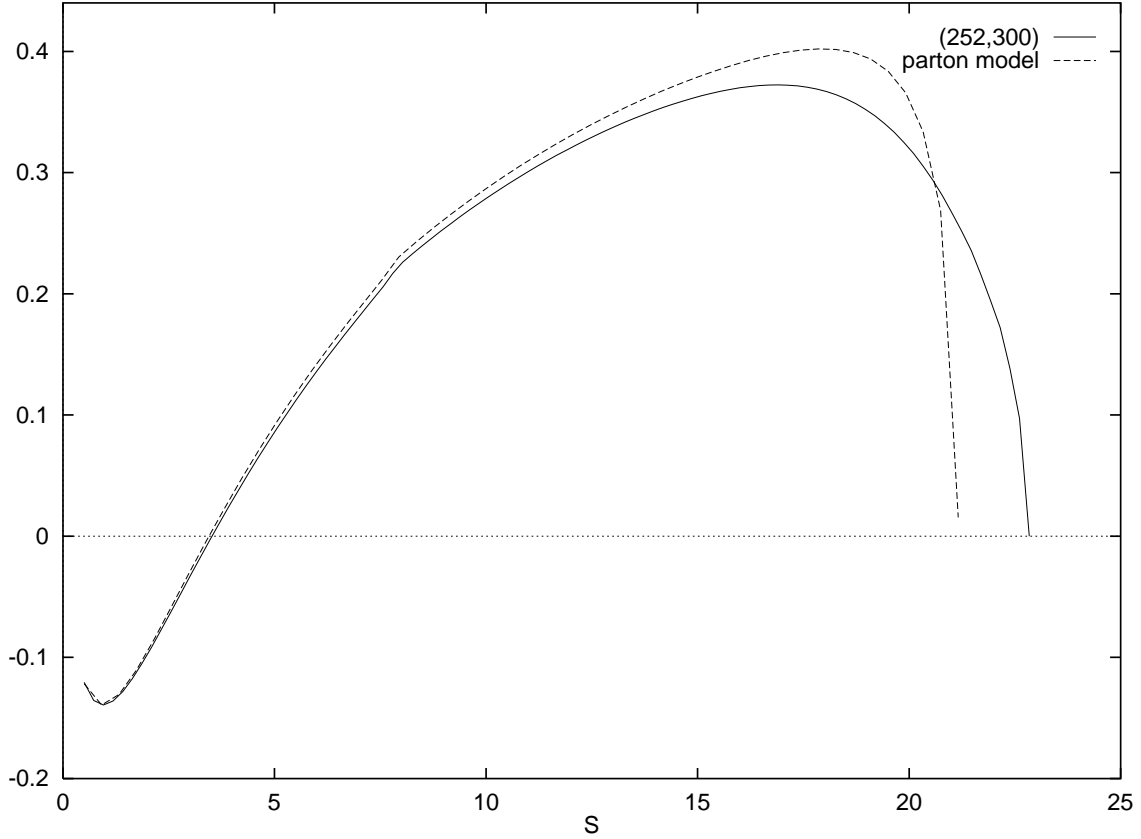


Figure 6: Normalized differential FB asymmetry  $d\bar{A}(s)/ds$  for  $B \rightarrow X_s \ell^+ \ell^-$  in the SM including the next-to-leading order QCD correction. The dashed curve corresponds to the parton model and the solid curve results from the Fermi motion model with the model parameters  $(p_F, m_q) = (252, 300)$  MeV, yielding an effective  $b$ -quark mass  $\langle W \rangle = 4.85$  GeV.

$(c\bar{c})$  continuum contribution, which we have already included in the coefficient  $C_9^{\text{eff}}$ , appear in the  $(\bar{s}_L \gamma_\mu b_L)(\bar{e} \gamma^\mu e)$  interaction term only, i.e. in the coefficient of the operator  $O_9$ . This implies that such LD-contributions should change  $C_9$  effectively, but keep  $C_7^{\text{eff}}$  and  $C_{10}$  unchanged. In principle, one has also a LD contribution in the effective coefficient  $C_7^{\text{eff}}$ ; this, however, has been discussed extensively in the context of the  $B \rightarrow X_s \gamma$  decay and estimated to be small [43, 44]. The LD-contribution is negligible in  $C_{10}$ . Hence, the three-coefficient fit of the data on  $B \rightarrow X_s \ell^+ \ell^-$  and  $B \rightarrow X_s \gamma$ , proposed in [35] on the basis of the SD-contributions, can be carried out also including the LD-effects. In accordance with this, to incorporate the LD-effects in  $B \rightarrow X_s \ell^+ \ell^-$ , the function  $Y(\hat{s})$  introduced earlier is replaced by,

$$Y(\hat{s}) \rightarrow Y'(\hat{s}) \equiv Y(\hat{s}) + Y_{\text{res}}(\hat{s}), \quad (57)$$

where  $Y_{\text{res}}(\hat{s})$  is given as [34],

$$Y_{\text{res}}(\hat{s}) = \frac{3}{\alpha^2} \kappa C^{(0)} \sum_{V_i=\psi(1s), \dots, \psi(6s)} \frac{\pi \Gamma(V_i \rightarrow l^+ l^-) M_{V_i}}{M_{V_i}^2 - \hat{s} m_b^2 - i M_{V_i} \Gamma_{V_i}}, \quad (58)$$

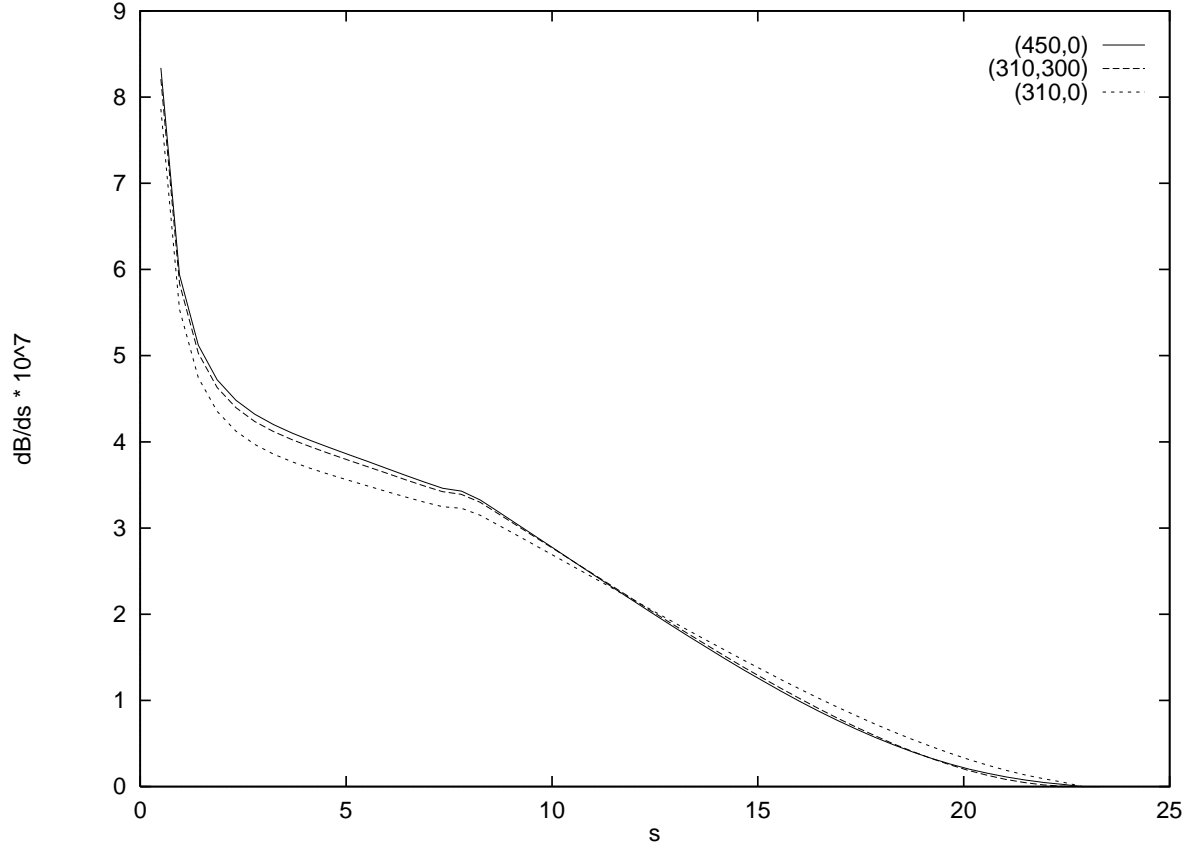


Figure 7: Differential branching ratio  $d\mathcal{B}/ds$  for  $B \rightarrow X_s \ell^+ \ell^-$  using the Fermi motion model for three different pairs of the model parameters  $(p_F, m_q) = (450, 0)$  MeV (solid curve),  $(310, 300)$  MeV (long dashed curve), and  $(310, 0)$  MeV (short dashed curve) yielding the effective  $b$ -quark masses  $\langle W \rangle = 4.76$  GeV, 4.80 GeV, and 4.92 GeV, respectively.

and

$$C^{(0)} \equiv 3C_1^{(0)} + C_2^{(0)} + 3C_3^{(0)} + C_4^{(0)} + 3C_5^{(0)} + C_6^{(0)}. \quad (59)$$

Here we adopt  $\kappa = 2.3$  for the numerical calculations [30]. Of course, the data determines only the combination  $\kappa C^{(0)} = 0.88$ . The relevant parameters of the charmonium resonances ( ${}^1S, \dots, {}^6S$ ) are given in the Particle Data Group [18], and we have averaged the leptonic widths for the decay modes  $V \rightarrow \ell^+ \ell^-$  for  $\ell = e$  and  $\ell = \mu$ . Note that in extrapolating the dilepton masses away from the resonance region, no extra  $q^2$ -dependence is included in the  $\gamma^*(q^2)$ - $V_i$  junction. (The  $q^2$ -dependence written explicitly in eq. (58) is due to the Breit-Wigner shape of the resonances.) This is an assumption and it may lead to an underestimate of the LD-effects in the low- $s$  region. However, as the present phenomenology is not equivocal on this issue, any other choice at this stage would have been on a similar footing. The resulting dilepton mass spectrum and the FB asymmetry are shown in Fig. 9 and Fig. 10, respectively. The two curves labeled SD and SD+LD include:

- Explicit  $O(\alpha_s)$ -improvement, calculated in the parton model [27, 28].

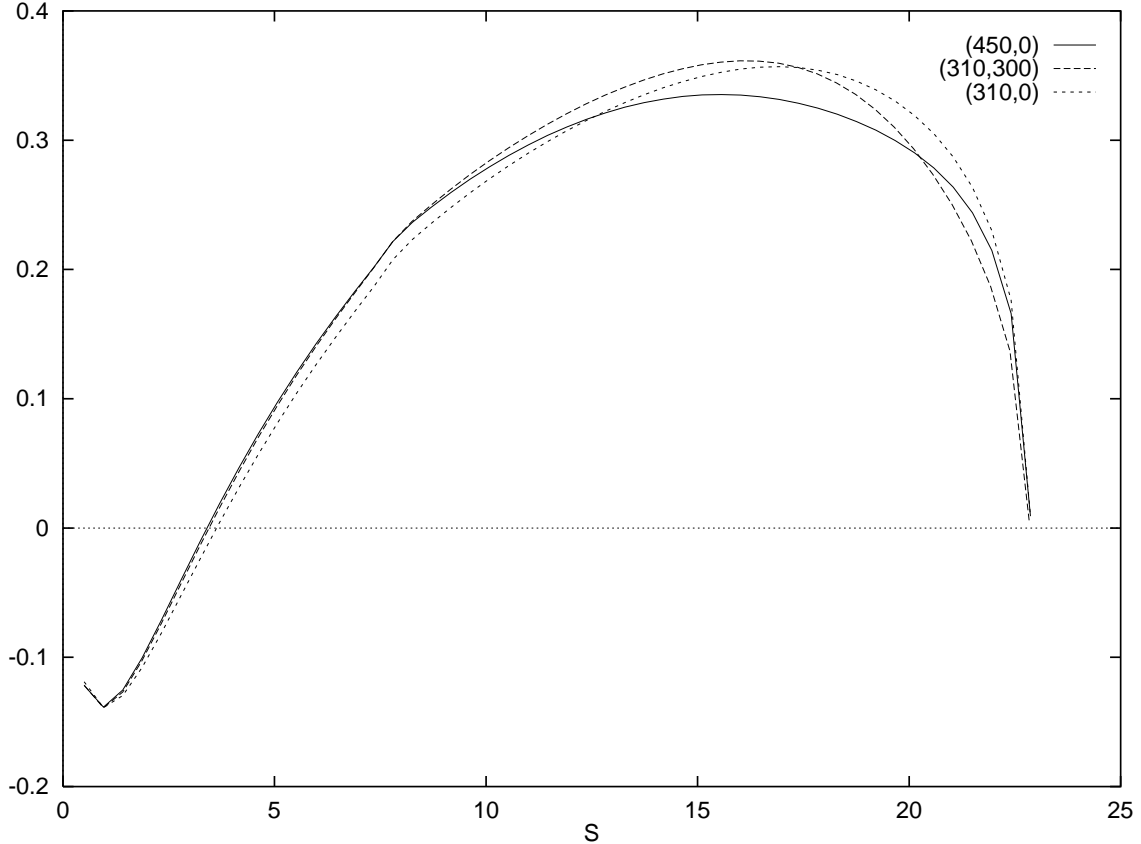


Figure 8: Normalized differential FB asymmetry  $d\bar{A}(s)/ds$  for  $B \rightarrow X_s \ell^+ \ell^-$  using the Fermi motion model for three different pairs of the model parameters  $(p_F, m_q) = (450, 0)$  MeV (solid curve),  $(310, 300)$  MeV (long dashed curve), and  $(p_F, m_q) = (310, 0)$  MeV (short dashed curve) yielding the effective  $b$ -quark masses  $\langle W \rangle = 4.76$  GeV, 4.80 GeV, and 4.92 GeV, respectively.

- Non-perturbative effects related with the bound state nature of the  $B$  hadrons and the physical threshold in the final state in  $B \rightarrow X_s \ell^+ \ell^-$ , using the Fermi motion model [22] with the parameters specified in the figures.

In addition, the SD+LD case also includes the LD-effects due to the vector resonances, contributing to  $C_9^{\text{eff}}$  as discussed earlier.

Finally, the parametric dependence due to the Fermi motion model is shown in Figs. 11 and 12 for the dilepton mass spectrum and the FB asymmetry, respectively, and compared with the case of the parton model in which case no wave-function effects are included. These figures give a fair estimate of the kind of uncertainties present in these distributions from non-perturbative effects. In particular, we draw attention to the marked dependence of the FB asymmetry to both the LD-(resonances) and wave function effects, which is particularly noticeable in the region  $m_{\ell\ell} > m(\psi')$ . The dilepton invariant mass spectrum, on the other hand, is very stable except at the very end of the spectrum, which is clearly different in all three cases shown.

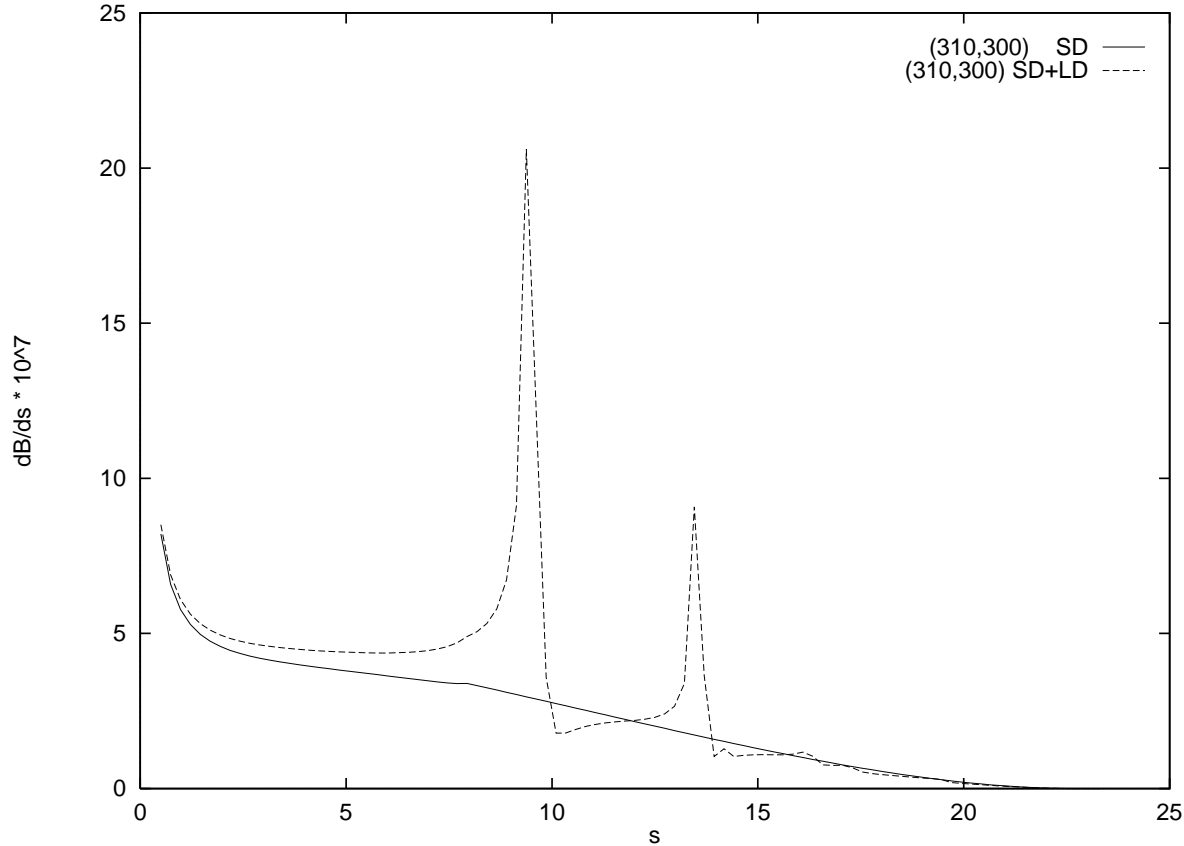


Figure 9: Differential branching ratio  $d\mathcal{B}/ds$  for  $B \rightarrow X_s \ell^+ \ell^-$  calculated in the SM using the next-to-leading order QCD corrections and Fermi motion effect (solid curve), and including the LD-contributions (dashed curve). The Fermi motion model parameters ( $P_F, m_q$ ) are displayed in the figure. Note that the height of the  $J/\psi$  peak is suppressed due to the linear scale.

## 5 Concluding Remarks

We have investigated the question of power corrections to the decay rates and distributions in the FCNC process  $B \rightarrow X_s \ell^+ \ell^-$  in the HQE framework. Our motivation here was to check if indeed the entire dilepton mass spectrum in these decays is calculable in a theoretically controlled sense, which the existing results suggested [33]. Our calculations of this distribution and the integrated rate do not agree with the ones obtained in FLS [33]. We have presented the details of our computations here, including the power corrections to the FB asymmetry not calculated earlier. In line with the analogous calculations for the lepton and photon energy spectra in radiative and semileptonic  $B$  decays, we have found that the HQE approach has a limited region of applicability in describing the dilepton mass spectrum in  $B \rightarrow X_s \ell^+ \ell^-$ . In the latter case, the use of the leading-order HQE approach in the high- $s$  region results in unphysical distribution and hence can not be used for comparison with data. Excluding the high- $s$  region, the power corrections to the dilepton mass spectrum and the FB asymmetry are, however, found to be small. The inclusive decay rate  $\Gamma(b \rightarrow s \ell^+ \ell^-)$  receives small power correction in

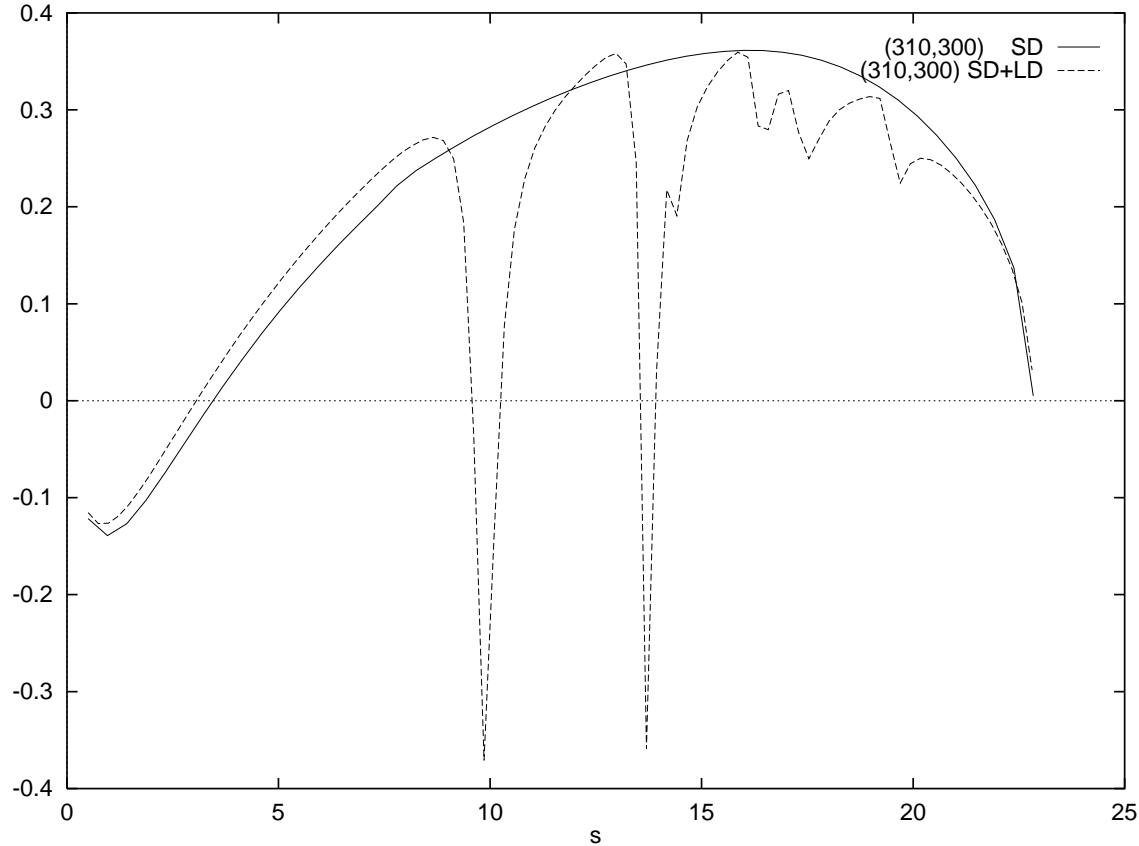


Figure 10: Normalized FB asymmetry  $\bar{A}(s)$  for  $B \rightarrow X_s \ell^+ \ell^-$  calculated in the SM using the next-to-leading order QCD corrections and Fermi motion effect (solid curve), and including the LD-contributions (dashed curve). The Fermi motion model parameters  $(P_F, m_q)$  are displayed in the figure.

the HQE approach, typically  $(-4\%)$ , which is similar to the one in the semileptonic decay width  $\Gamma(b \rightarrow u \ell \nu_\ell)$  but not identical.

Despite progress in some sectors, the problem of incorporating non-perturbative effects in weak decays remains theoretically an intractable problem. In the present context, the structure functions  $T_i$ 's entering the decay distributions in  $B \rightarrow X_s \ell^+ \ell^-$  are not known from first principles in QCD. We have modeled the non-perturbative effects in  $B \rightarrow X_s \ell^+ \ell^-$  using a popular Fermi motion model [22], which allows to incorporate  $B$ -hadron wave function effects and the correct threshold in the final states. Since this model gives a good description of the existing data on the lepton and photon energy spectra in  $B$  decays [9, 23], we hope that it describes similar non-perturbative effects in the decay  $B \rightarrow X_s \ell^+ \ell^-$  as well. We have estimated the dispersion on the theoretical predictions for the dilepton mass and the FB asymmetry resulting from the present uncertainty in the model parameters. This dispersion is marked in the high dilepton mass region in the FB asymmetry, but the dilepton mass spectrum is remarkably stable. Hence, in the very high- $s$  region, non-perturbative effects are important and have to be

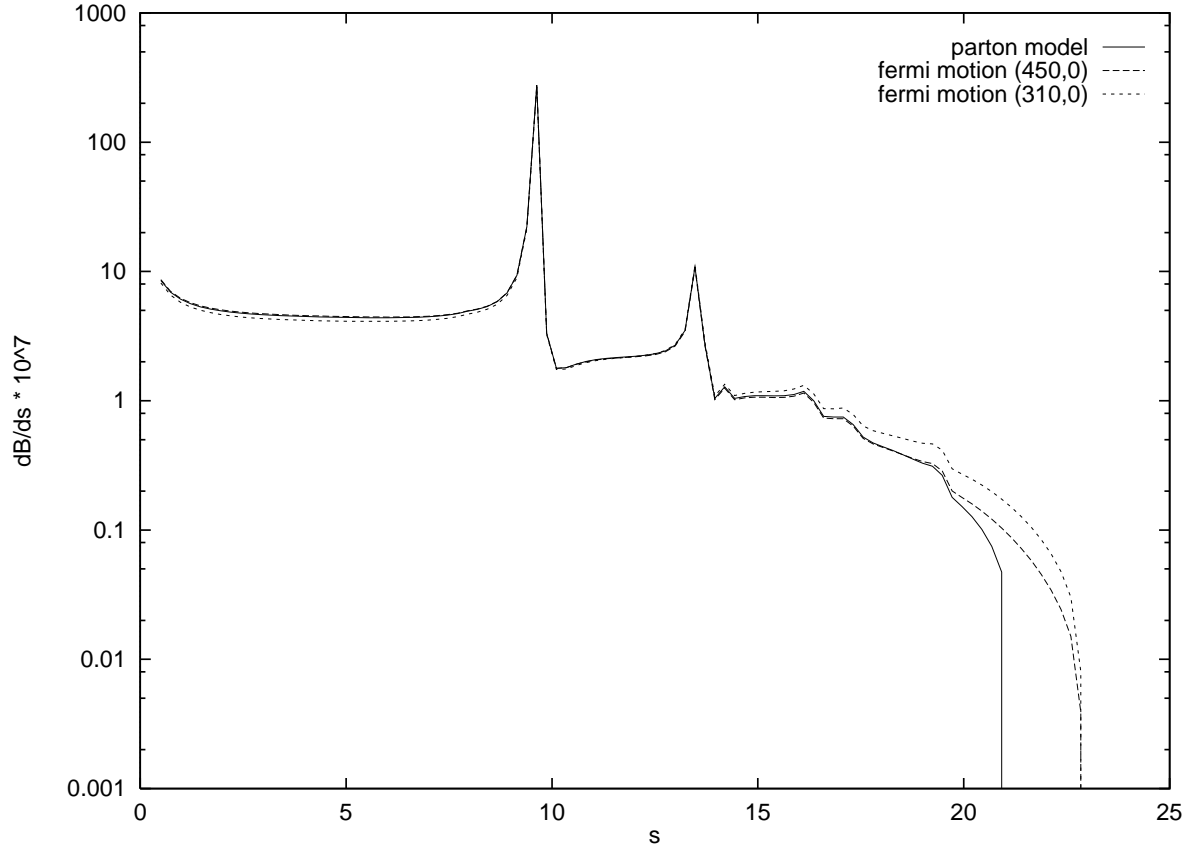


Figure 11: Dilepton invariant mass distribution in  $B \rightarrow X_s \ell^+ \ell^-$  in the SM including next-to-leading order QCD correction and LD effects. The solid curve corresponds to the parton model and the short-dashed and long-dashed curves correspond to including the Fermi motion effects. The values of the Fermi motion model are indicated in the figure.

included in order to have a reliable comparison of the SM-based distributions and data, as and when they become available.

Finally, we have incorporated the LD-effects using data in  $B$  decays and the measured properties of the resonances in the charmonium sector. As discussed in the literature, this is not sufficient to uniquely determine the dilepton distributions away from these resonances. In that context, we note that the vector-meson-dominance (VMD) approximation of the old vintage [45] is often invoked to model the  $q^2$ -dependence of the  $\gamma$ - $V$  junction,  $g_V(q^2)$ . This VMD-framework has been used to estimate the LD-effects in  $B \rightarrow X_s \gamma$  [44]. Theoretical uncertainties from these aspects in the dilepton mass distributions in  $B \rightarrow X_s \ell^+ \ell^-$  have been discussed in [32]. We hope that data from HERA on the photoproduction of  $J/\psi$  and  $\psi'$  (and other resonances) can be used to implement the  $q^2$ -dependence of the effective vertices to eliminate (or at least reduce) the present theoretical uncertainty from this source. However, as the HERA-data on the relevant processes  $\gamma^*(q^2) + p \rightarrow J/\psi(\psi') + p$  are still preliminary and a  $q^2$ -dependence has not yet quantitatively been extracted [46], we do not attempt to

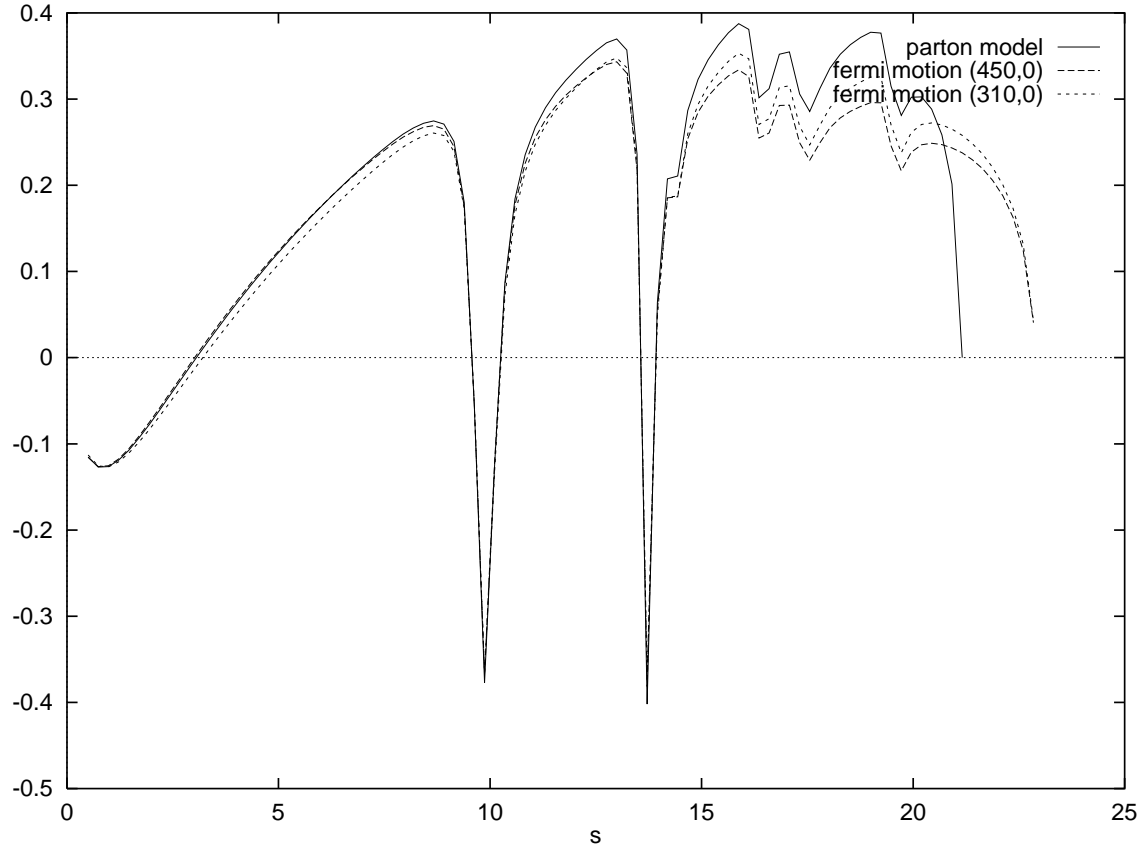


Figure 12: FB asymmetry for  $B \rightarrow X_s \ell^+ \ell^-$  in the SM as a function of the dimuon invariant mass including the next-to-leading order QCD correction and LD effects. The solid curve corresponds to the parton model and the short-dashed and long-dashed curves correspond to including the Fermi motion effects. The values of the Fermi motion model are indicated in the figure.

undertake an improved treatment of the LD-effects in  $B \rightarrow X_s \ell^+ \ell^-$  here. In view of this, and the remaining theoretical uncertainties on the perturbative part discussed in section 3, the distributions shown in Figs. (11) and (12) have an overall uncertainty of order  $\pm 25\%$ .

## Acknowledgements

We thank Christoph Greub for helpful discussions and correspondence on implementing the Fermi motion effects. L.T.H. and T.M. would like to thank C.S. Kim, T. Onogi, M. Tanaka and A. Yamada for useful discussions. L.T.H. would also like to thank the theory group at KEK for the warm hospitality during his stay at KEK. The work of L.T.H. is supported by a grant from the Ministry of Education, Science and Culture (Mombusho), Japan. The research work of T.M. has been partially supported by the Deutscher Akademischer Austausch Dienst (DAAD) and the Japan Society for the Promotion of Science (JSPS), which made a visit to DESY-Hamburg possible, where this work was completed.

## Appendices

### A The functions $T_i^{(j)}(v \cdot \hat{q}, \hat{s})$

In this appendix we list the expressions for the decomposition of the structure functions  $T_i(v \cdot \hat{q}, \hat{s})$ , ( $i = 1, 2, 3$ ) in terms of the functions  $T_i^{(j)}(v \cdot \hat{q}, \hat{s})$ , with  $j = 0, 1, 2, s, g, \delta$ , representing the power corrections in  $b \rightarrow s\ell^+\ell^-$  up to and including terms of order  $M_B/m_b^3$  and explicitly keeping the  $s$ -quark mass dependence. The origin of these individual terms is explained in the text. The parton model contributions  $T_i^{(0)}$  are given in eqs. (A-1) - (A-3).

$$\begin{aligned} T_1^{(0)L/R} = & -\frac{1}{x} \frac{M_B}{m_b} \left\{ (1 - v \cdot \hat{q}) |C_9^{\text{eff}} \mp C_{10}|^2 \right. \\ & + \frac{4}{\hat{s}^2} \left[ (1 + \hat{m}_s^2) (2(v \cdot \hat{q})^2 - \hat{s}(v \cdot \hat{q}) - \hat{s}) - 2\hat{m}_s^2 \hat{s} \right] |C_7^{\text{eff}}|^2 \\ & \left. + \frac{4}{\hat{s}} [v \cdot \hat{q} - \hat{s} - \hat{m}_s^2(v \cdot \hat{q})] \text{Re}[(C_9^{\text{eff}} \mp C_{10})^* C_7^{\text{eff}}] \right\}, \end{aligned} \quad (\text{A-1})$$

$$T_2^{(0)L/R} = -\frac{2}{x} \frac{M_B}{m_b} \left\{ |C_9^{\text{eff}} \mp C_{10}|^2 - \frac{4}{\hat{s}} (1 + \hat{m}_s^2) |C_7^{\text{eff}}|^2 \right\}, \quad (\text{A-2})$$

$$\begin{aligned} T_3^{(0)L/R} = & \frac{1}{x} \frac{M_B}{m_b} \left\{ -|C_9^{\text{eff}} \mp C_{10}|^2 - \frac{4}{\hat{s}^2} [2(v \cdot \hat{q}) - \hat{s}] [1 - \hat{m}_s^2] |C_7^{\text{eff}}|^2 \right. \\ & \left. - \frac{4}{\hat{s}} (\hat{m}_s^2 + 1) \text{Re}[(C_9^{\text{eff}} \mp C_{10})^* C_7^{\text{eff}}] \right\}, \end{aligned} \quad (\text{A-3})$$

$$\begin{aligned} T_1^{(1)L/R} = & -\frac{1}{3} \frac{M_B}{m_b^3} (\lambda_1 + 3\lambda_2) \left\{ \left[ \frac{1}{x} - \frac{2}{x^2} (\hat{s} - (v \cdot \hat{q})^2) \right] |C_9^{\text{eff}} \mp C_{10}|^2 \right. \\ & + \frac{4}{\hat{s}^2} \left[ \frac{1}{x} (\hat{s} - 2(v \cdot \hat{q})^2) - \frac{2}{x^2} (\hat{s}^2 - 2\hat{s}(v \cdot \hat{q}) - \hat{s}(v \cdot \hat{q})^2 + 2(v \cdot \hat{q})^3) \right] (1 + \hat{m}_s^2) |C_7^{\text{eff}}|^2 \\ & \left. - (\hat{s} - v \cdot \hat{q}^2) \hat{m}_s^2 \frac{8}{\hat{s}x^2} \text{Re}(C_9^{\text{eff}} \mp C_{10})^* C_7^{\text{eff}} \right\}, \end{aligned} \quad (\text{A-4})$$

$$T_2^{(1)L/R} = -\frac{2}{3} \frac{M_B}{m_b^3} (\lambda_1 + 3\lambda_2) \left[ \frac{1}{x} + \frac{2}{x^2} v \cdot \hat{q} \right] \left[ -|C_9^{\text{eff}} \mp C_{10}|^2 + \frac{4}{\hat{s}} (1 + \hat{m}_s^2) |C_7^{\text{eff}}|^2 \right], \quad (\text{A-5})$$

$$\begin{aligned} T_3^{(1)L/R} = & -\frac{2}{3} \frac{M_B}{m_b^3} (\lambda_1 + 3\lambda_2) \left\{ \frac{1}{x^2} (1 - v \cdot \hat{q}) |C_9^{\text{eff}} \mp C_{10}|^2 \right. \\ & - \frac{4}{\hat{s}^2} \left[ \frac{1}{x} v \cdot \hat{q} - \frac{1}{x^2} (\hat{s} + \hat{s}(v \cdot \hat{q}) - 2(v \cdot \hat{q})^2) \right] (1 - \hat{m}_s^2) |C_7^{\text{eff}}|^2 \\ & \left. - v \cdot \hat{q} \hat{m}_s^2 \frac{4}{\hat{s}x^2} \text{Re}(C_9^{\text{eff}} \mp C_{10})^* C_7^{\text{eff}} \right\}, \end{aligned} \quad (\text{A-6})$$

$$\begin{aligned} T_1^{(2)L/R} = & \frac{1}{3} \frac{M_B}{m_b^3} \lambda_1 \left\{ \left[ -\frac{4}{x^3} (\hat{s} - (v \cdot \hat{q})^2) + \frac{3}{x^2} \right] (1 - v \cdot \hat{q}) |C_9^{\text{eff}} \mp C_{10}|^2 \right. \\ & - \frac{4}{\hat{s}^2 x^3} \left[ -4\hat{s}^2 - 12\hat{m}_s^2 \hat{s}^2 + 3\hat{s}x + 9\hat{m}_s^2 \hat{s}x - 4\hat{s}^2 v \cdot \hat{q} - 4\hat{m}_s^2 \hat{s}^2 v \cdot \hat{q} + 7\hat{s}xv \cdot \hat{q} \right. \\ & \left. + 7\hat{m}_s^2 \hat{s}xv \cdot \hat{q} + 12\hat{s}v \cdot \hat{q}^2 + 20\hat{m}_s^2 \hat{s}v \cdot \hat{q}^2 - 6xv \cdot \hat{q}^2 - 6\hat{m}_s^2 xv \cdot \hat{q}^2 + 4\hat{s}v \cdot \hat{q}^3 \right] \end{aligned}$$

$$\begin{aligned}
& + 4\hat{m}_s^2 v \cdot \hat{q}^3 \hat{s} - 4xv \cdot \hat{q}^3 - 4\hat{m}_s^2 xv \cdot \hat{q}^3 - 8v \cdot \hat{q}^4 - 8\hat{m}_s^2 v \cdot \hat{q}^4 \Big] |C_7^{\text{eff}}|^2 \\
& + \frac{4}{\hat{s}x^3} \left[ 4\hat{s}^2 - 5\hat{s}x - 4\hat{s}v \cdot \hat{q} + 4\hat{m}_s^2 \hat{s}v \cdot \hat{q} + 3xv \cdot \hat{q} - 3\hat{m}_s^2 xv \cdot \hat{q} - 4\hat{s}v \cdot \hat{q}^2 + 2xv \cdot \hat{q}^2 \right. \\
& \left. + 4v \cdot \hat{q}^3 - 4\hat{m}_s^2 v \cdot \hat{q}^3 \right] \text{Re} \left[ (C_9^{\text{eff}} \mp C_{10})^* C_7^{\text{eff}} \right] \Big\} , \tag{A-7}
\end{aligned}$$

$$\begin{aligned}
T_2^{(2)L/R} &= -\frac{2}{3} \frac{M_B}{m_b^3} \lambda_1 \left[ \frac{4}{x^3} \left( \hat{s} - (v \cdot \hat{q})^2 \right) - \frac{3}{x^2} - \frac{2}{x^2} v \cdot \hat{q} \right] \\
&\quad \left( |C_9^{\text{eff}} \mp C_{10}|^2 - \frac{4}{\hat{s}} (1 + \hat{m}_s^2) |C_7^{\text{eff}}|^2 \right) , \tag{A-8}
\end{aligned}$$

$$\begin{aligned}
T_3^{(2)L/R} &= -\frac{1}{3} \frac{M_B}{m_b^3} \lambda_1 \left\{ \left[ \frac{4}{x^3} \left( \hat{s} - (v \cdot \hat{q})^2 \right) - \frac{5}{x^2} \right] |C_9^{\text{eff}} \mp C_{10}|^2 \right. \\
&\quad \left. + \frac{4}{\hat{s}^2 x^3} \left[ -4\hat{s}^2 + 5\hat{s}x + 8\hat{s}v \cdot \hat{q} - 6xv \cdot \hat{q} + 4\hat{s}v \cdot \hat{q}^2 - 4xv \cdot \hat{q}^2 - 8v \cdot \hat{q}^3 \right] (1 - \hat{m}_s^2) |C_7^{\text{eff}}|^2 \right. \\
&\quad \left. + \frac{4}{\hat{s}x^3} \left[ (4\hat{s} - 3x - 4v \cdot \hat{q}^2)(1 + \hat{m}_s^2) - 2xv \cdot \hat{q} \right] \text{Re} \left[ (C_9^{\text{eff}} \mp C_{10})^* C_7^{\text{eff}} \right] \right\} , \tag{A-9}
\end{aligned}$$

$$T_1^{(s)L/R} = \frac{2}{\hat{s}x} \frac{M_B}{m_b^3} (\lambda_1 + 3\lambda_2) \left[ (\hat{s} - v \cdot \hat{q}) \text{Re} \left[ (C_9^{\text{eff}} \mp C_{10})^* C_7^{\text{eff}} \right] + 2\hat{m}_s^2 |C_7^{\text{eff}}|^2 \right] , \tag{A-10}$$

$$T_2^{(s)L/R} = 0 , \tag{A-11}$$

$$T_3^{(s)L/R} = -\frac{2}{\hat{s}x} \frac{M_B}{m_b^3} (\lambda_1 + 3\lambda_2) \text{Re} \left[ (C_9^{\text{eff}} \mp C_{10})^* C_7^{\text{eff}} \right] , \tag{A-12}$$

$$\begin{aligned}
T_1^{(g)L/R} &= \frac{1}{x^2} \frac{M_B}{m_b^3} \lambda_2 \left\{ -(1 - v \cdot \hat{q}) |C_9^{\text{eff}} \mp C_{10}|^2 \right. \\
&\quad \left. + \frac{4}{\hat{s}^2} \left[ \hat{s} + 3\hat{m}_s^2 \hat{s} + \hat{s}(v \cdot \hat{q})(1 + \hat{m}_s^2) - 2(v \cdot \hat{q})^2 (1 + \hat{m}_s^2) \right] |C_7^{\text{eff}}|^2 \right. \\
&\quad \left. + \frac{4}{\hat{s}} (\hat{s} - v \cdot \hat{q} (1 - \hat{m}_s^2)) \text{Re} \left[ (C_9^{\text{eff}} \mp C_{10})^* C_7^{\text{eff}} \right] \right\} , \tag{A-13}
\end{aligned}$$

$$T_2^{(g)L/R} = \frac{-2}{x^2} \frac{M_B}{m_b^3} \lambda_2 \left\{ -|C_9^{\text{eff}} \mp C_{10}|^2 - \frac{4}{\hat{s}} (1 + \hat{m}_s^2) |C_7^{\text{eff}}|^2 - 4 \text{Re} \left[ (C_9^{\text{eff}} \mp C_{10})^* C_7^{\text{eff}} \right] \right\} , \tag{A-14}$$

$$\begin{aligned}
T_3^{(g)L/R} &= \frac{-1}{x^2} \frac{M_B}{m_b^3} \lambda_2 \left\{ |C_9^{\text{eff}} \mp C_{10}|^2 + \frac{4}{\hat{s}^2} [2(v \cdot \hat{q}) - \hat{s}] (1 - \hat{m}_s^2) |C_7^{\text{eff}}|^2 \right. \\
&\quad \left. + \frac{4}{\hat{s}} (1 + \hat{m}_s^2) \text{Re} \left[ (C_9^{\text{eff}} \mp C_{10})^* C_7^{\text{eff}} \right] \right\} , \tag{A-15}
\end{aligned}$$

$$\begin{aligned}
T_1^{(\delta)L/R} &= \frac{1}{2} \frac{M_B}{m_b^3} (\lambda_1 + 3\lambda_2) \left\{ \left[ \frac{1}{x} - \frac{2}{x^2} (1 - v \cdot \hat{q})^2 \right] |C_9^{\text{eff}} \mp C_{10}|^2 \right. \\
&\quad \left. - \frac{4}{\hat{s}^2 x^2} \left[ -2\hat{s} - 6\hat{m}_s^2 \hat{s} + \hat{s}x + \hat{m}_s^2 \hat{s}x + 4\hat{m}_s^2 \hat{s}v \cdot \hat{q} + 4v \cdot \hat{q}^2 + 4\hat{m}_s^2 v \cdot \hat{q} + 2\hat{s}v \cdot \hat{q}^2 \right. \right. \\
&\quad \left. \left. + 2\hat{m}_s^2 \hat{s}v \cdot \hat{q}^2 - 2xv \cdot \hat{q}^2 - 2\hat{m}_s^2 xv \cdot \hat{q}^2 - 4v \cdot \hat{q}^3 - 4\hat{m}_s^2 v \cdot \hat{q}^3 \right] |C_7^{\text{eff}}|^2 \right. \\
&\quad \left. - \frac{4}{\hat{s}x^2} \left[ -2\hat{s} + 2v \cdot \hat{q} - 2\hat{m}_s^2 v \cdot \hat{q} + 2\hat{s}v \cdot \hat{q} - xv \cdot \hat{q} - 2v \cdot \hat{q}^2 \right. \right. \\
&\quad \left. \left. + 2\hat{m}_s^2 v \cdot \hat{q}^2 \right] \text{Re} \left[ (C_9^{\text{eff}} \mp C_{10})^* C_7^{\text{eff}} \right] \right\} , \tag{A-16}
\end{aligned}$$

$$T_2^{(\delta)L/R} = \frac{M_B}{m_b^3} (\lambda_1 + 3\lambda_2) \left[ \frac{1}{x} - \frac{2}{x^2} (1 - v \cdot \hat{q}) \right] \left[ |C_9^{\text{eff}} \mp C_{10}|^2 - \frac{4}{\hat{s}} (1 + \hat{m}_s^2) |C_7^{\text{eff}}|^2 \right] , \tag{A-17}$$

$$T_3^{(\delta)L/R} = \frac{M_B}{m_b^3} (\lambda_1 + 3\lambda_2) \left\{ -\frac{1}{x^2} (1 - v \cdot \hat{q}) |C_9^{\text{eff}} \mp C_{10}|^2 \right. \tag{A-18}$$

$$\begin{aligned}
& + \frac{4}{\hat{s}^2} \left[ \frac{1}{x} v \cdot \hat{q} - \frac{1}{x^2} (1 - v \cdot \hat{q}) (2(v \cdot \hat{q}) - \hat{s}) \right] (1 - \hat{m}_s^2) |C_7^{\text{eff}}|^2 \\
& - \frac{2}{\hat{s}x^2} \left[ 2 + 2\hat{m}_s^2 - x - 2v \cdot \hat{q} - 2\hat{m}_s^2 v \cdot \hat{q} \right] \text{Re} \left[ (C_9^{\text{eff}} \mp C_{10})^* C_7^{\text{eff}} \right] \}.
\end{aligned} \quad (\text{A-18})$$

In the above expressions, the variable  $x$  is defined as  $x \equiv 1 + \hat{s} - 2(v \cdot \hat{q}) - \hat{m}_s^2 + i\epsilon$ .

## B Auxiliary functions $E_1(\hat{s}, \hat{u})$ and $E_2(\hat{s}, \hat{u})$ in the Dalitz distribution $d^2\mathcal{B}/d\hat{s}d\hat{u}(b \rightarrow s\ell^+\ell^-)$ in the HQE Approach

In this appendix we give the auxiliary functions  $E_1(\hat{s}, \hat{u})$  and  $E_2(\hat{s}, \hat{u})$ , multiplying the delta-function  $\delta[\hat{u}(\hat{s}, \hat{m}_s) - \hat{u}^2]$  and its first derivative  $\delta'[\hat{u}(\hat{s}, \hat{m}_s) - \hat{u}^2]$ , respectively, appearing in the power corrected Dalitz distribution in  $b \rightarrow s\ell^+\ell^-$  given in eq. (41) in the text.

$$\begin{aligned}
E_1(\hat{s}, \hat{u}) = & \frac{1}{3} \left\{ 2\hat{\lambda}_1 \left[ 1 - 4\hat{m}_s^2 + 6\hat{m}_s^4 - 4\hat{m}_s^6 + \hat{m}_s^8 - 2\hat{m}_s^2\hat{s} + 4\hat{m}_s^4\hat{s} - 2\hat{m}_s^6\hat{s} + 2\hat{m}_s^2\hat{s}^3 - \hat{s}^4 \right. \right. \\
& + \hat{u}^2 \left( 1 - 2\hat{m}_s^2 + \hat{m}_s^4 - 2\hat{m}_s^2\hat{s} + 4\hat{s} + \hat{s}^2 \right) \left. \right] \\
& + 3\hat{\lambda}_2 (1 - \hat{m}_s^2 + \hat{s}) \left[ -1 + 7\hat{m}_s^2 - 11\hat{m}_s^4 + 5\hat{m}_s^6 + 11\hat{s} + 10\hat{m}_s^2\hat{s} - 5\hat{m}_s^4\hat{s} - 15\hat{s}^2 \right. \\
& - 5\hat{m}_s^2\hat{s}^2 + 5\hat{s}^3 + \hat{u}^2 \left( 1 - 5\hat{m}_s^2 + 5\hat{s} \right) \left. \right] \left\} \right. \\
& \times \left( |C_9^{\text{eff}}|^2 + |C_{10}|^2 \right) \\
& + \frac{4}{3\hat{s}} \left\{ 2\hat{\lambda}_1 \left[ 1 - 3\hat{m}_s^2 + 2\hat{m}_s^4 + 2\hat{m}_s^6 - 3\hat{m}_s^8 + \hat{m}_s^{10} - 10\hat{m}_s^2\hat{s} + 18\hat{m}_s^4\hat{s} - 6\hat{m}_s^6\hat{s} - 2\hat{m}_s^8\hat{s} \right. \right. \\
& + 16\hat{m}_s^4\hat{s}^2 - 6\hat{m}_s^2\hat{s}^3 + 2\hat{m}_s^4\hat{s}^3 - \hat{s}^4 - \hat{m}_s^2\hat{s}^4 \\
& - \hat{u}^2 \left( 1 - \hat{m}_s^2 - \hat{m}_s^4 + \hat{m}_s^6 + 4\hat{s} + 2\hat{m}_s^2\hat{s} - 2\hat{m}_s^4\hat{s} + \hat{s}^2 + \hat{m}_s^2\hat{s}^2 \right) \left. \right] \\
& + 3\hat{\lambda}_2 (1 - \hat{m}_s^2 + \hat{s}) \left[ 3 + 2\hat{m}_s^2 - 8\hat{m}_s^4 - 2\hat{m}_s^6 + 5\hat{m}_s^8 + 3\hat{s} - 35\hat{m}_s^2\hat{s} - 27\hat{m}_s^4\hat{s} - 5\hat{m}_s^6\hat{s} \right. \\
& - 11\hat{s}^2 + 8\hat{m}_s^2\hat{s}^2 - 5\hat{m}_s^4\hat{s}^2 + 5\hat{s}^3 + 5\hat{m}_s^2\hat{s}^3 \\
& + \hat{u}^2 \left( 3 + 8\hat{m}_s^2 + 5\hat{m}_s^4 - 5\hat{s} - 5\hat{m}_s^2\hat{s} \right) \left. \right] \left\} |C_7^{\text{eff}}|^2 \\
& + 8 \left\{ \frac{2}{3} \hat{\lambda}_1 (1 - 4\hat{m}_s^2 + 6\hat{m}_s^4 - 4\hat{m}_s^6 + \hat{m}_s^8 - \hat{s} - \hat{m}_s^2\hat{s} + 5\hat{m}_s^4\hat{s} - 3\hat{m}_s^6\hat{s} + \hat{s}^2 + 3\hat{m}_s^4\hat{s}^2 \right. \\
& - \hat{s}^3 - \hat{m}_s^2\hat{s}^3) \\
& + \hat{\lambda}_2 (1 - \hat{m}_s^2 + \hat{s}) \left[ 4 - 3\hat{m}_s^2 - 6\hat{m}_s^4 + 5\hat{m}_s^6 - 6\hat{s} - 4\hat{m}_s^2\hat{s} - 10\hat{m}_s^4\hat{s} + 2\hat{s}^2 + 5\hat{m}_s^2\hat{s}^2 + \hat{u}^2 \right] \left. \right\} \\
& \text{Re}(C_9^{\text{eff}}) C_7^{\text{eff}} \\
& + 4\hat{s}\hat{u} \left[ -\frac{4}{3}\hat{\lambda}_1\hat{s} + \hat{\lambda}_2 \left( 7 - 2\hat{m}_s^2 - 5\hat{m}_s^4 + 2\hat{s} + 10\hat{m}_s^2\hat{s} - 5\hat{s}^2 \right) \right] \text{Re}(C_9^{\text{eff}}) C_{10} \\
& + \frac{8}{3}\hat{u} \left[ -4\hat{\lambda}_1\hat{s} (1 + \hat{m}_s^2) \right]
\end{aligned}$$

$$+3\hat{\lambda}_2 \left( 5 + \hat{m}_s^2 - \hat{m}_s^4 - 5\hat{m}_s^6 + 2\hat{s} + 4\hat{m}_s^2\hat{s} + 10\hat{m}_s^4\hat{s} - 3\hat{s}^2 - 5\hat{m}_s^2\hat{s}^2 \right) \right] C_{10}^* C_7^{\text{eff}}, \quad (\text{B-1})$$

$$\begin{aligned} E_2(\hat{s}, \hat{u}) = & \frac{2}{3} \hat{\lambda}_1 \left( 1 - \hat{m}_s^2 + \hat{s} \right)^2 \hat{u}(\hat{s}, \hat{m}_s)^2 \left[ \left( 1 - 2\hat{m}_s^2 + \hat{m}_s^4 - \hat{s}^2 - \hat{u}^2 \right) \left( |C_9^{\text{eff}}|^2 + |C_{10}|^2 \right) \right. \\ & + 4 \left( 1 - \hat{m}_s^2 - \hat{m}_s^4 + \hat{m}_s^6 - 8\hat{m}_s^2\hat{s} - \hat{s}^2 - \hat{m}_s^2\hat{s}^2 + \hat{u}^2 + \hat{m}_s^2\hat{u}^2 \right) \frac{|C_7^{\text{eff}}|^2}{\hat{s}} \\ & + 8 \left( 1 - 2\hat{m}_s^2 + \hat{m}_s^4 - \hat{s} - \hat{m}_s^2\hat{s} \right) \text{Re}(C_9^{\text{eff}}) C_7^{\text{eff}} \\ & \left. + 4\hat{s}\hat{u} \text{Re}(C_9^{\text{eff}}) C_{10} + 8\hat{u}(1 + \hat{m}_s^2) \text{Re}(C_{10}) C_7^{\text{eff}} \right] \\ & . \end{aligned} \quad (\text{B-2})$$

## C The decay rate $\Gamma(b \rightarrow s\ell^+\ell^-)$ in the $V - A$ limit and comparison with the existing results

In this appendix we compare our results for the power corrections in the decay  $B \rightarrow X_s\ell^+\ell^-$  with the ones for the decays  $B \rightarrow X_c\ell\nu_\ell$ , derived by Manohar and Wise (MW) [16]. In doing this, we shall reduce the matrix element for the decay  $B \rightarrow X_s\ell^+\ell^-$  to the one encountered in  $B \rightarrow X_c\ell\nu_\ell$ , obtained by the replacements:

$$C_9 = -C_{10} = \frac{1}{2}, \quad (\text{C-1})$$

$$C_7 = 0, \quad (\text{C-2})$$

$$\left( \frac{G_F \alpha}{\sqrt{2} \pi} V_{ts}^* V_{tb} \right) \rightarrow \left( -\frac{4 G_F}{\sqrt{2}} V_{cb} \right). \quad (\text{C-3})$$

This amounts to keeping only the CC  $V - A$  contribution in  $B \rightarrow X_s\ell^+\ell^-$ .

We remark that our hadronic states and the ones used by Manohar and Wise are differently normalized, with the two related by

$$|M\rangle = \sqrt{2M_B} |M\rangle^{MW}. \quad (\text{C-4})$$

Hence, the forward scattering amplitudes are related through,

$$T_{\mu\nu} = -\frac{1}{2M_B} T_{\mu\nu}^{MW}. \quad (\text{C-5})$$

Likewise, the matrix elements of the kinetic energy and the magnetic moment operators in the HQE approach are related,

$$\lambda_1 = -2m_b^2 K_b, \quad (\text{C-6})$$

$$3\lambda_2 = -2m_b^2 G_b, \quad (\text{C-7})$$

$$\lambda_1 + 3\lambda_2 = -2m_b^2 E_b = -2m_b^2 (K_b + G_b). \quad (\text{C-8})$$

Note further that our structure functions  $T_i$  are dimensionless, as opposed to the ones employed in [16]. Thus,

$$(T_1)^{MW} = -\frac{(T_1)}{2M_B}, \quad (C-9)$$

$$(T_2)^{MW} = -\frac{(T_2)}{2M_B}, \quad (C-10)$$

$$(T_3)^{MW} = -\frac{(T_3)}{2M_B m_b}. \quad (C-11)$$

With these replacements, the structure functions  $T_i$ ,  $i = 1, 2, 3$  given in the text and Appendix A in this paper agree with those in MW up to the indicated normalization factors in the  $V - A$  limit. Note that the function  $\Delta_0$  defined in eq. (3.4) of [16] transcribes to  $\Delta_0 = m_b^2 x$  in our notation, with  $x$  defined in Appendix A.

After integrating  $T_{\mu\nu} L^{\mu\nu}$  in the complex  $v \cdot \hat{q}$  plane, we have also compared the double differential distribution  $(1/\Gamma_b) d\Gamma/dy d\hat{q}^2$ , given in eq. (5.2) of [16]. Taking into account that our differential distributions are defined in terms of the variables  $\hat{u}$  and  $\hat{s}$ , as opposed to the variables  $\hat{s}$  and  $y$  with  $y \equiv 2 \hat{E}_e$  used in [16], and making the variable transformation  $y = \hat{u} - 2 v \cdot \hat{q}$ , we reproduce their result.

Finally, using the correspondence (C-1) - (C-3), the differential dilepton distribution in  $b \rightarrow s\ell^+\ell^-$  reduces to (with  $m_s = 0$ )

$$\frac{d\Gamma}{d\hat{s}} = \Gamma^b \left( \frac{1}{3} (1 - \hat{s})^2 (1 + 2\hat{s}) (2 + \hat{\lambda}_1) + (1 - 15\hat{s}^2 + 10\hat{s}^3) \hat{\lambda}_2 \right), \quad (C-12)$$

which, on integration gives

$$\Gamma = \Gamma^b \left( 1 + \frac{1}{2} \hat{\lambda}_1 - \frac{9}{2} \hat{\lambda}_2 \right), \quad (C-13)$$

where  $\Gamma^b$  is the parton model decay width. The above expression agrees with the well known result of Bigi et al [15]. Doing the same manipulation on the corresponding expressions by FLS [33], we get instead

$$\Gamma^{FLS} = \Gamma^b \left( 1 + \frac{17}{3} \hat{\lambda}_1 + 13 \hat{\lambda}_2 \right), \quad (C-14)$$

where in  $\Gamma^{FLS}$  also only the  $V - A$  contributions are kept. This disagrees with our result as well as with the one in [15].

## D Equivalence of FB Asymmetry and Energy Asymmetry in $B \rightarrow X_s \ell^+ \ell^-$

In this appendix we address a peripheral issue, namely that the quantity Energy asymmetry, introduced in [36], is simply related to the FB asymmetry, defined in [34, 35], and is not an independent quantity. It is easy to show that the configuration in which  $\ell^+$  is scattered in the forward direction, measured with respect to the direction of the  $B$ -meson momentum in the dilepton c.m.s., corresponds to the events in which  $E_- > E_+$  in the  $B$ -meson rest frame, where  $E_\pm$  represents the  $\ell^\pm$ -energy. To that end let us suppose that in the dilepton c.m.s.,  $\ell^+$  is scattered in the forward direction. In this frame, the four-momenta of  $\ell^+$  and  $\ell^-$  are given as

$$p_\mu^+ = (\epsilon, p_{\parallel}, p_{\perp}) , \quad (\text{D-1})$$

$$p_\mu^- = (\epsilon, -p_{\parallel}, -p_{\perp}) , \quad (\text{D-2})$$

where  $p_{\parallel} > 0$  is the longitudinal momentum and  $p_{\perp}$  is the transverse momentum. Boosting the momenta with the velocity of  $B$  meson ( $v$ ) takes one to the  $B$ -meson rest frame, where  $E_+$  and  $E_-$ , are given by

$$E_+ = \epsilon \frac{1}{\sqrt{1-v^2}} - p_{\parallel} \frac{v}{\sqrt{1-v^2}} , \quad (\text{D-3})$$

$$E_- = \epsilon \frac{1}{\sqrt{1-v^2}} + p_{\parallel} \frac{v}{\sqrt{1-v^2}} . \quad (\text{D-4})$$

implying that for forward scattered  $\ell_+$  in the dilepton c.m.s., one has  $E_+ < E_-$  in the  $B$  meson rest frame. By using the definition of the FB-asymmetry in [34, 35], we obtain the following simple relation to the energy asymmetry of [36],

$$\frac{d\mathcal{A}(\hat{s})}{d\hat{s}} = \int_0^1 \frac{d^2\mathcal{B}}{d\hat{s} dz} dz - \int_{-1}^0 \frac{d^2\mathcal{B}}{d\hat{s} dz} dz , \quad (\text{D-5})$$

where  $z \equiv \cos \theta$ ,

$$\int \frac{d\mathcal{A}(\hat{s})}{d\hat{s}} d\hat{s} = \mathcal{B} \times A , \quad (\text{D-6})$$

where  $A \equiv [N(E_- > E_+) - N(E_+ > E_-)]/[N(E_- > E_+) + N(E_+ > E_-)]$  is the energy asymmetry defined in [36]. Hence  $A$  of [36] is identical to the normalized FB asymmetry  $\bar{A}$  calculated in this paper. That the two quantities are related can also be seen by writing the Mandelstam

variable  $\hat{u}$ , defined previously, in the dilepton c.m.s. and the  $B$ -meson rest frame:

$$\begin{aligned}\hat{u} &= -\hat{u}(\hat{s}) \cos \theta \\ &= 2(\hat{E}_+ - \hat{E}_-).\end{aligned}\quad (\text{D-7})$$

## E Dalitz distribution $d^2\Gamma(B \rightarrow X_s \ell^+ \ell^-)/dsdu$ and FB asymmetry in the Fermi motion model

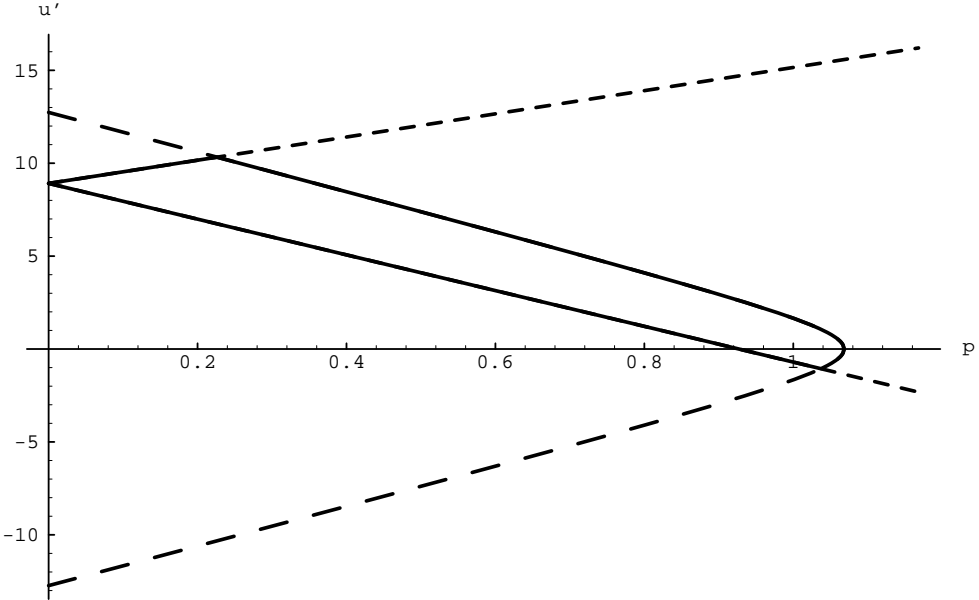


Figure 13: Phase space boundaries for the  $u'$  and  $p$  integrations with fixed values of  $s$  and  $u$  drawn for  $s = 15 \text{ GeV}^2$  and  $u = 8.9 \text{ GeV}^2$ . The integration region (solid curve) is given by the intersection of  $u'_\pm$  (short dashed) and  $\pm u(s, p)$  (long dashed curve). The fermi motion parameters used are  $(p_F, m_q) = (450, 0)$ .

We start with the differential decay rate  $d^3\Gamma_B/ds du dp$ , describing the decay  $b \rightarrow s \ell^+ \ell^-$  of a moving  $b$ -quark having a mass  $W(p)$  and three momentum  $|p| \equiv p$  with a distribution  $\phi(p)$ , which will be taken as a Gaussian [22],

$$\frac{d\Gamma_B}{ds du dp} = \int_{u'_{\min}}^{u'_{\max}} du' \frac{W(p)^2}{M_B} p \phi(p) \frac{1}{\sqrt{u'^2 + 4 W(p)^2 s}} \left[ \frac{d^2\Gamma_b}{ds du'} \right]. \quad (\text{E-1})$$

Here,  $d^2\Gamma_b/ds du'$  is the double differential decay rate of a  $b$ -quark at rest and can be written in the case of  $b \rightarrow s \ell^+ \ell^-$  as,

$$\frac{d^2\Gamma_b}{ds du'} = |V_{ts} V_{tb}|^2 \frac{G_F^2}{192 \pi^3} \frac{1}{W(p)^3} \frac{3 \alpha^2}{16 \pi^2} [F_1(s, p) + F_2(s, p) u' + F_3(s, p) u'^2], \quad (\text{E-2})$$

and the three functions have the following expressions,

$$\begin{aligned}
F_1(s, p) = & \left[ (W(p)^2 - m_s^2)^2 - s^2 \right] \left( |C_9^{\text{eff}}|^2 + |C_{10}|^2 \right) \\
& + 4 \left[ W(p)^4 - m_s^2 W(p)^2 - m_s^4 + \frac{m_s^6}{W(p)^2} - 8 s m_s^2 - s^2 \left( 1 + \frac{m_s^2}{W(p)^2} \right) \right] \frac{W(p)^2}{s} |C_7^{\text{eff}}|^2 \\
& - 8 \left[ s (W(p)^2 + m_s^2) - (W(p)^2 - m_s^2)^2 \right] \text{Re}(C_7^{\text{eff}} C_9^{\text{eff}}), \tag{E-3}
\end{aligned}$$

$$F_2(s, p) = 4 s \text{Re}(C_9^{\text{eff}} C_{10}) + 8 (W(p)^2 + m_s^2) C_{10} C_7^{\text{eff}}, \tag{E-4}$$

$$F_3(s, p) = - \left( |C_9^{\text{eff}}|^2 + |C_{10}|^2 \right) + 4 \left[ 1 + \left( \frac{m_s^2}{W(p)^2} \right)^2 \right] \frac{W(p)^2}{s} |C_7^{\text{eff}}|^2, \tag{E-5}$$

which can be read off directly from eq. (41) in the limit  $\lambda_i = 0$ ;  $i = 1, 2$ . Note that the Wilson coefficient  $C_9^{\text{eff}}$  also has an implicit  $W(p)$  dependence, as can be seen in the text. The integration limit for  $u'$  is determined through the equations

$$u'_{\max} \equiv \text{Min} [u'_+, u(s, p)], \tag{E-6}$$

$$u'_{\min} \equiv \text{Max} [u'_-, -u(s, p)], \tag{E-7}$$

where

$$u'_{\pm} \equiv \frac{E_W}{M_B} u \pm \frac{p}{M_B} \sqrt{4 s M_B^2 + u^2}, \tag{E-8}$$

$$E_W = \sqrt{W(p)^2 + p^2}, \tag{E-9}$$

and

$$u(s, p) \equiv \sqrt{[s - (W(p) + m_s)^2] [s - (W(p) - m_s)^2]}. \tag{E-10}$$

A typical situation in the phase space is displayed in Fig. 13. Integration over  $p$  gives the double differential decay rate (Dalitz distribution) including the Fermi motion. The result is,

$$\begin{aligned}
\frac{d^2\Gamma_B}{ds du} = & |V_{ts} V_{tb}|^2 \frac{G_F^2}{192 \pi^3} \frac{3 \alpha^2}{16 \pi^2} \int_0^{p_{\max}} dp \frac{1}{W(p)^3} \frac{W(p)^2}{2M_B} p \phi(p) \\
& \left\{ F_1(s, p) \log \left| \frac{u'_{\max} + \sqrt{u'_{\max}^2 + 4 W(p)^2 s}}{u'_{\min} + \sqrt{u'_{\min}^2 + 4 W(p)^2 s}} \right| \right. \\
& + F_2(s, p) \left[ \sqrt{u'_{\max}^2 + 4 W(p)^2 s} - \sqrt{u'_{\min}^2 + 4 W(p)^2 s} \right] \\
& + F_3(s, p) \frac{1}{2} \left[ u'_{\max} \sqrt{u'_{\max}^2 + 4 W(p)^2 s} - u'_{\min} \sqrt{u'_{\min}^2 + 4 W(p)^2 s} \right. \\
& \left. \left. - 4 W(p)^2 s \log \left| \frac{u'_{\max} + \sqrt{u'_{\max}^2 + 4 W(p)^2 s}}{u'_{\min} + \sqrt{u'_{\min}^2 + 4 W(p)^2 s}} \right| \right] \right\}. \tag{E-11}
\end{aligned}$$

Note that the upper limit in  $p$  integration,  $p_{\max}$  is determined such that  $p$  satisfies,

$$u'_{\max}(p_{\max}, s, u) = u'_{\min}(p_{\max}, s, u) . \quad (\text{E-12})$$

Lastly, the normalized differential FB asymmetry including the Fermi motion becomes,

$$\frac{d\bar{A}}{ds} = \frac{\int_{-u_{\text{ph}}}^0 \frac{d\Gamma_B}{ds du} du - \int_0^{u_{\text{ph}}} \frac{d\Gamma_B}{ds du} du}{\int_{-u_{\text{ph}}}^0 \frac{d\Gamma_B}{ds du} du + \int_0^{u_{\text{ph}}} \frac{d\Gamma_B}{ds du} du} , \quad (\text{E-13})$$

where

$$u_{\text{ph}} \equiv \sqrt{\left[s - (M_B + M_X)^2\right] \left[s - (M_B - M_X)^2\right]} , \quad (\text{E-14})$$

and

$$M_X \equiv \text{Max} [m_K, m_s + m_q] , \quad (\text{E-15})$$

with  $m_q$  the spectator quark mass and  $m_K$  the kaon mass. Since the calculations are being done for an inclusive decay  $B \rightarrow X_s \ell^+ \ell^-$ , we should have put this threshold higher, say starting from  $m_K + m_\pi$ , but as this effects the very end of a steeply falling dilepton mass spectrum, we have kept the threshold in  $B \rightarrow X_s \ell^+ \ell^-$  at  $m(X_s) = m_K$ .

## References

- [1] S.L. Glashow, J. Iliopoulos, and L. Maiani, Phys. Rev. **D2** (1970) 1285.
- [2] N. Cabibbo, Phys. Rev. Lett. **10** (1963) 531; M. Kobayashi and T. Maskawa, Prog. Theor. Phys. **49** (1973) 652.
- [3] R. Ammar et al. (CLEO Collaboration), Phys. Rev. Lett. **71** (1993) 674.
- [4] M.S. Alam et al. (CLEO Collaboration), Phys. Rev. Lett. **74** (1995) 2885.
- [5] M. Ciuchini et al., Phys. Lett. **B316** (1993) 127; Nucl. Phys. **B415** (1994) 403; G. Cella et al., Phys. Lett. **B325** (1994) 227; M. Misiak, Nucl. Phys. **B393** (1993) 23 [E. **B439** (1995) 461].
- [6] A.J. Buras, M. Misiak, M. Münz, and S. Pokorski, Nucl. Phys. **B424** (1994) 374.
- [7] M. Ciuchini et al., Phys. Lett. **B334** (1994) 137.
- [8] A. Ali and C. Greub, Z. Phys. **C49** (1991) 431; Phys. Lett. **B259** (1991) 182; Z. Phys. **C60** (1993) 433.
- [9] A. Ali and C. Greub, Phys. Lett. **B361** (1995) 146.
- [10] N. Pott, Phys. Rev. **D54** (1996) 938.
- [11] G. Korchemsky and G. Sterman, Phys. Lett. **B340** (1994) 96.
- [12] R.D. Dikeman, M. Shifman and R.G. Uraltsev, Int. J. Mod. Phys. **A11** (1996) 571.
- [13] C. Greub, T. Hurth and D. Wyler, Phys. Lett. **B380** (1996) 385; Phys. Rev. **D54** (1996) 3350.
- [14] K.G. Chetyrkin, M. Misiak, and M. Münz (to be published); reported by M. Misiak at the Int. Conf. on High Energy Physics, Warsaw, July 25 - 31, 1996.
- [15] J. Chay, H. Georgi and B. Grinstein, Phys. Lett. **B247** (1990) 399; I.I. Bigi, N.G. Uraltsev and A.I. Vainshtein, Phys. Lett. **B293** (1992) 430 [E. **B297** (1993) 477]; I.I. Bigi et al., Phys. Rev. Lett. **71** (1993) 496; B. Blok et al., Phys. Rev. **D49** (1994) 3356 [E. **D50** (1994) 3572].

- [16] A. Manohar and M. B. Wise, Phys. Rev. **D49** (1994) 1310.
- [17] A. Ali, DESY Report 96-106 [hep-ph/9606324]; to appear in: *Proceedings of the XX International Summer College on Physics and Contemporary Needs*, Bhurban, Pakistan, June 24 - July 13, 1995 (Nova Science Publishers, New York).
- [18] R.M. Barnett et al. (Particle Data Group), Phys. Rev. **D54** (1996) 1.
- [19] I. Bigi et al., Int. J. Mod. Phys., **A9** (1994) 2467.
- [20] A. Falk et al., Phys. Rev. **D49** (1994) 4553.
- [21] R. Jaffe and L. Randall, Nucl. Phys. **B412** (1994) 79.
- [22] A. Ali and E. Pietarinen, Nucl. Phys. **B154** (1979) 519; G. Altarelli et al., Nucl. Phys. **B208** (1982) 365.
- [23] M. Barish et al. (CLEO Collaboration), Phys. Rev. Lett. **76** (1996) 1570; Ed. Thorndike (private communication).
- [24] C. Greub and S.-J. Rey, preprint SLAC-PUB-7245 [hep-ph/9608247].
- [25] M. Neubert, Phys. Rev. **D49** (1994) 4623.
- [26] B. Grinstein, M.J. Savage and M.B. Wise, Nucl. Phys. **B319** (1989) 271.
- [27] M. Misiak in ref. [5].
- [28] A.J. Buras and M. Münz, Phys. Rev. **D52** (1995) 186.
- [29] C. S. Lim, T. Morozumi and A. I. Sanda, Phys. Lett. **218** (1989) 343; N. G. Deshpande, J. Trampetic and K. Panose, Phys. Rev. **D39** (1989) 1461; P. J. O'Donnell and H. K. K. Tung, Phys. Rev. **D43** (1991) R2067; N. Paver and Riazuddin, Phys. Rev. **D45** (1992) 978.
- [30] Z. Ligeti and M.B. Wise, Phys. Rev. **D53** (1996) 4937.
- [31] F. Krüger and L.M. Sehgal, Phys. Lett. **B380** (1996) 199.
- [32] M.R. Ahmady, Phys. Rev. **D53** (1996) 2843.

- [33] A. F. Falk, M. Luke and M. J. Savage, Phys. Rev. **D49** (1994) 3367.
- [34] A. Ali, T. Mannel and T. Morozumi, Phys. Lett. **B273** (1991) 505.
- [35] A. Ali, G. F. Giudice and T. Mannel, Z. Phys. **C67** (1995) 417.
- [36] P. Cho, M. Misiak and D. Wyler, Phys. Rev. **D54** (1996) 3329.
- [37] M. Jeżabek and J. H. Kühn, Nucl. Phys. **B320** (1989) 20.
- [38] M. Luke, Phys. Lett. **B252** (1990) 447; A.F. Falk and M. Neubert, Phys. Rev. **D47** (1993) 2965.
- [39] P. Ball and V.M. Braun, Phys. Rev. **D49** (1994) 2472; V. Eletsky and E. Shuryak, Phys. Lett. **B276** (1992) 191; M. Neubert, Phys. Lett. **B322** (1994) 419.
- [40] M. Neubert, preprint CERN-TH/96-208 [hep-ph/9608211].
- [41] Z. Ligeti and Y. Nir, Phys. Rev. **D49** (1994) 4331; M. Gremm, A. Kapustin, Z. Ligeti and M.B. Wise, Phys. Rev. Lett. **77** (1996) 20; A. F. Falk, M. Luke and M. J. Savage, Phys. Rev. **D53** (1996) 6316; V. Chernyak, preprint Budker INP-96-23 (1996) [hep-ph/9604376].
- [42] K. Fujikawa and A. Yamada, Phys. Rev. **D49** (1994) 5890.
- [43] J.M. Soares, Phys. Rev. **D53** (1996) 241; J. Milana, Phys. Rev. **D53** (1996) 1403; G. Ricciardi, Phys. Lett. **B355** (1995) 313; E. Golowich and S. Pakvasa, Phys. Rev. **D51**, 1215 (1995).
- [44] N.G. Deshpande, X.-G. He, and J. Trampetic, Phys. Lett. **B367** (1996) 362. See also, G. Eilam et al., preprint TECHNION-PH-95-18 (1995).
- [45] K. Terasaki, Nuovo Cim. **66A** (1981) 475.
- [46] “High  $Q^2$  exclusive vector meson production at HERA” (ZEUS Collaboration), contributed paper pa02-028, XXVIII Int. Conf. on High Energy Physics, Warsaw, July 25 - 31, 1996.